ESA contract N° 4000106390/12/NL/LF

20737/KaSAR/D6/FR

Technical Assistance for the Deployment of Airborne-Based Ka-band SAR and Geophysical Measurements during the KaSAR 2012 Campaign

KaSAR final report

February 15th, 2013

	Auteurs	Verified by	Approved by
Fonction	Research engineer	Project manager	Director
Nom	X Dupuis, JF Nouvel P Dubois-Fernandez	P Dubois-Fernandez	
Visa	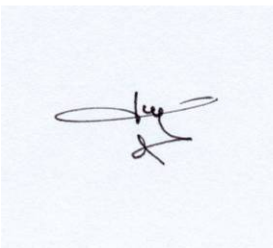	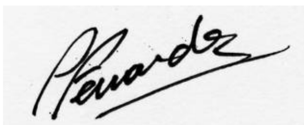	

KaSAR Final Report

Acronyms and reference documents

Ref	Document
REF-1	Contract KA-SAR2012 - TBD
REF-2	Statement of Work for Technical Assistance for the Deployment of Airborne-based Ka-Band SAR and geo-physical measurements during the KaSAR 2012 Campaign – EOP-SM-2345-RB-ag
REF-3	Response to request for proposal : Ka-SAR2012 campaign – ONERA/DEMR/TBD
REF-4	RAMSES data archive analysis report – 20737/KaSAR/WP1/D2/V2
REF-5	Data Acquisition Report – 20737/KaSAR/D3/V1
REF-6	Handbook of Radar Scattering Statistics for terrain, F. T. Ulaby and M. C. Dobson.
REF-7	Gamma0 curve at Ka Band for small vegetation provided by E. Attema

Acronym	Meaning
BUSARD	Banc Ultra-léger pour Systèmes Aéroportés de Recherche sur les Drones
CEV	Centre d’Essai en Vol
DEMR	Département ElectroMagnétisme et Radar
HF	Hyper-Frequency
IFMCW	Interrupted Frequency Modulation Continuous Wave
ISLR	Integrated Side Lobe Ratio
NE-Sigma0	Noise-Equivalent Sigma0
Pamela	ONERA/DEMR SAR processing tool
PSLR	Peak to Side Lobe Ratio
RF	Radio-Frequency
SAR	Synthetic Aperture Radar

1. Introduction

This document constitutes the final report of the KaSAR-2012 project [ESA Contract N°4000106390/12/NL/LF].

To support feasibility studies for a spaceborne high-resolution single-satellite interferometric SAR system operating in Ka-band and the associated technology roadmap, a better knowledge of Ka-band backscatter levels of natural targets as a function of incidence angles is required.

More specifically, the KaSAR-2012 campaign [REF-2] is proposed to provide feedbacks to ESA on

- ⇨ Radiometry of Ka-band over natural medium reflectivity surfaces (i.e. bare soil, forest, grass/agriculture fields) as a function of incidence angle from 20° to 50°.
- ⇨ Dynamic range of Ka-band signal (Radar Cross-sections) over targets of very high (anthropogenic bright targets), medium (bare soil, vegetation) and low (flat inner waters or runways) reflectivity
- ⇨ Signature variability as a function of time-varying environmental conditions over selected land (wet and dry) and water (smooth and rough) surfaces
- ⇨ Variability and information content of Ka-band at different polarisations
- ⇨ Ka-band signature over hard targets (boats, vehicles) and infrastructure targets (pipelines, power lines, train tracks, etc.) for sizes, shapes and structural target characterisation

The above objectives have been addressed through a set of coordinated ground and airborne SAR acquisitions over sites located in Southern France and analysis over both the BUSARD-DRIVE processed datasets and the 2008 RAMSES archive dataset acquired at Ka bands.

The report contains two main sections. The first one is dedicated to the analysis of archive data acquired in June 2008 by RAMSES, the ONERA sensor onboard a Transall. The second part is dedicated to the analysis of the Ka Band data, acquired in the context of this study with the ONERA DRIVE-BUSARD instrument on board a Stemme motorglider. Both sections are organised in parallel structures with a processing and calibration section followed by an analysis of the backscattering behaviour for natural targets (agricultural fields, sea), industrial and urban areas, and anthropogenic targets.

2. Ramses Archive data analysis

2.1. Description of the dataset

Data from the RAMSES archive in Ka band were acquired for the French MoD in June 2008. Acquisitions took place in the South of France over St Gilles and Port la Nouvelle.

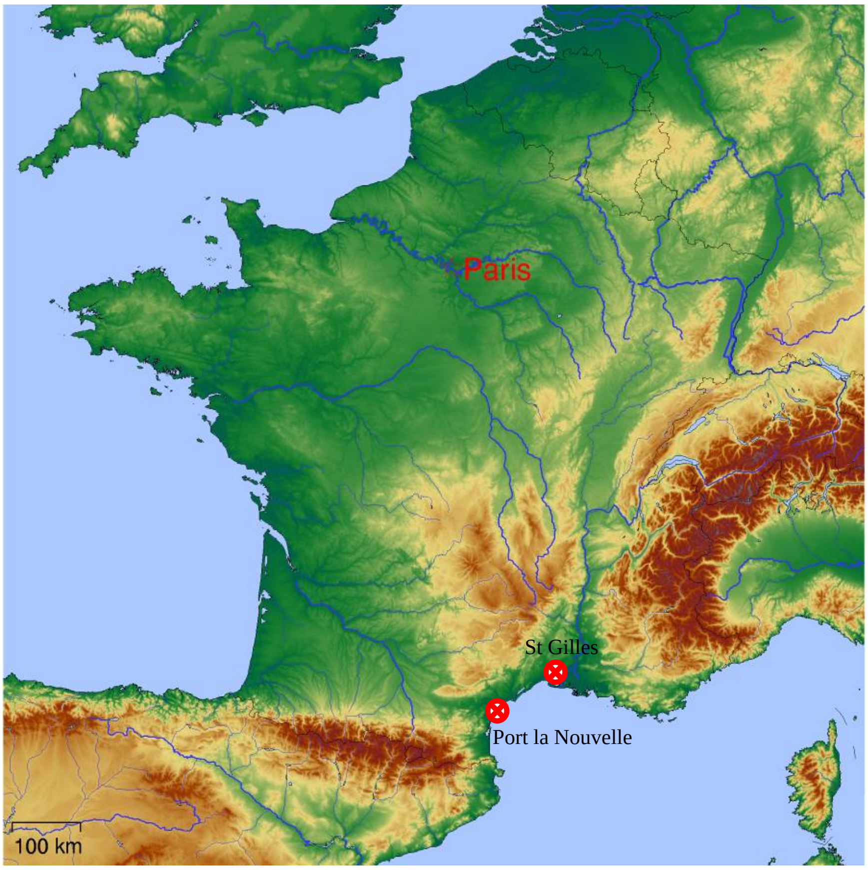

Figure 1 : location of imaged area.

The imaged scenes are composed of the coastal town and surroundings of Port la Nouvelle and of St Gilles agricultural landscape. The data were acquired in very high resolution (VHR: 1.22 GHz bandwidth) and in high resolution (HR: 620 MHz bandwidth) with a central frequency of 34.920GHz for both resolutions. Table 1 summarizes the main system parameters for RAMSES used during the acquisition campaign.

Parameters	VHR	HR
Central frequency	34,920 GHz	
wave form	Step Frequency	Step Frequency
number of chirp	4	2
PRF	19531,25 Hz	9920,63 Hz
Sampling rate	800 MHz	
Bandwidth	1,220 GHz	620 MHz

Table 1 : summary of the system parameters

For each acquisition several corners reflectors were deployed for calibration purpose, in the images presented in this section they are located in the red rectangles. Table 2 lists the data in the RAMSES archive in Ka band and their parameters.

	Polarization	Resolution	incidence angle	Imaged area
SA0602	Hh	VHR	40°	Port la Nouvelle
SA0603	Hh	HR	40°	Port la Nouvelle
SA0605	Hh	VHR	60°	Port la Nouvelle
SA0610	Hh	VHR	40°	St Gilles
SA0611	Vv	VHR	40°	St Gilles

Table 2 : available Ka band images in the Ramses archive.

2.1.1. St Gilles area

2.1.1.1. SA0610, VHR, Hh polarization, incidence angle of 40°

Figure 2 : SA0610 very high resolution Ka image of St Gilles area in Hh polarization for 40° incidence angle. The red rectangle localizes the corner reflectors.

2.1.1.2. SA0611, VHR, Vv polarization, incidence angle of 40°

Figure 3 : SA0611 very high resolution Ka image of St Gilles area in Vv polarization for 40° incidence angle. The red rectangle localizes the corner reflectors.

2.1.2. Port la nouvelle area

2.1.2.1. SA0602, VHR, Hh polarization, incidence angle of 40°

Figure 4 : SA0602 very high resolution Ka image of Port la Nouvelle area in Hh polarization for 40° incidence angle. The red rectangle localizes the corner reflectors.

2.1.2.2. SA0603, HR, Hh polarization, incidence angle of 40°

Figure 5 : SA0603 high resolution Ka image of Port la Nouvelle area in Hh polarization for 40° incidence angle. The red rectangle localizes the corner reflectors.

2.1.2.3. SA0605, VHR, Hh polarization, incidence angle of 60°

Figure 6 : SA0605 very high resolution Ka image of Port la Nouvelle area in Hh polarization for 60° incidence angle. The red rectangle localizes the corner reflectors.

2.2.Calibration analysis

In this section the calibration quality is analyzed. Corner reflectors of different sizes,(**Figure 7**, **Figure 8**, Table 3) were deployed for each area. The back-scattering response, value and curves, of the reflectors are given for each image. Furthermore, an upper bound for the NE-Sigma0 is measured in the darkest areas of the image.

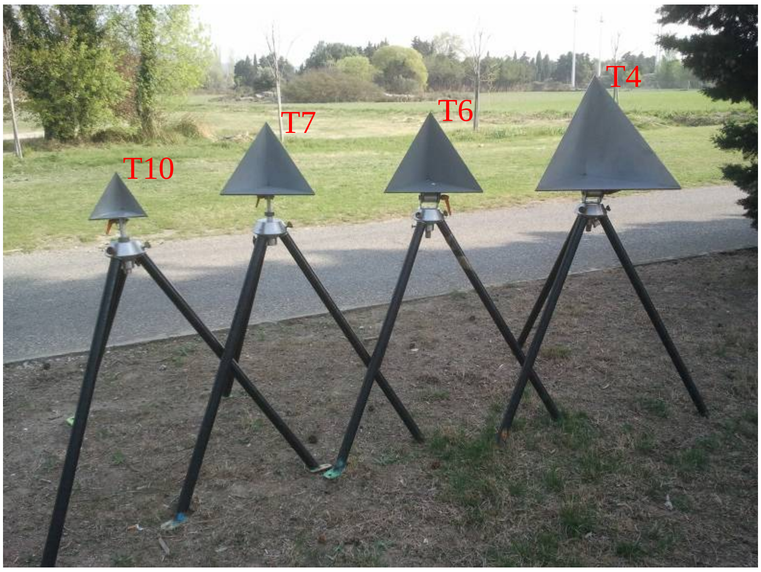

Figure 7 : set of Ka corner reflectors

Figure 8 : corner reflector deployment in Port la Nouvelle

Table 3 summarizes the size and the theoretical value in dB for each corner reflector deployed during the acquisitions.

Corner reflector	size (m)	Theo RCS (dB)
T10	0,125	11,4
T9	0,149	14,4
T8	0,177	17,4
T7	0,222	21,4
T6	0,264	24,4
T5	0,314	27,4
T4	0,395	31,4

Table 3 : Size and theoretical values (in dB) of the corner reflectors deployed for this acquisition campaign.

2.2.1. SA0610, VHR, Hh polarization, incidence angle of 40°

Figure 9 : corner reflector area for SA610

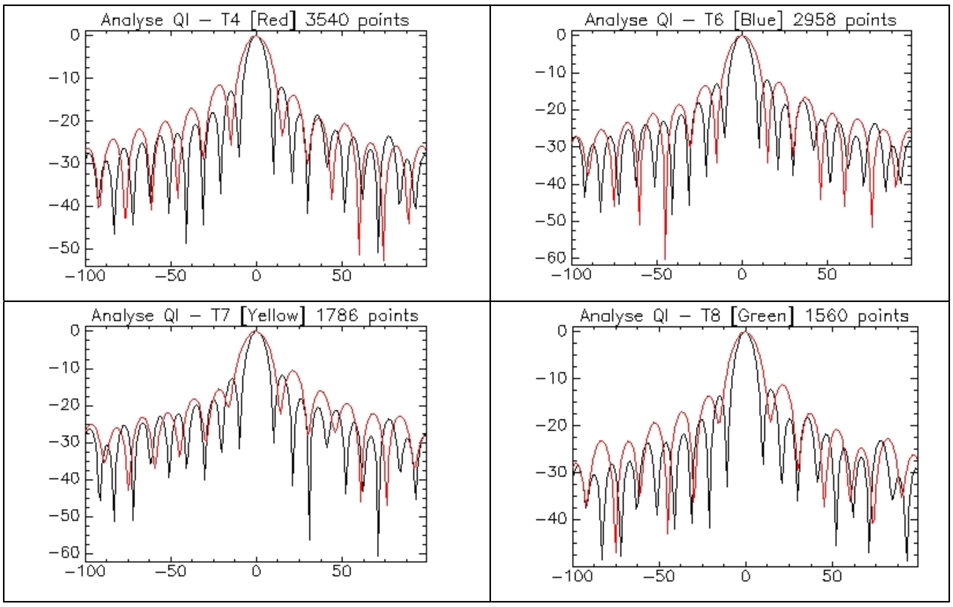

Figure 10 : response of the different corner reflectors along slant range direction in black and azimuth direction in red. Abscise is over-sampled Pixel (by 8).

One calibration key is then estimated for each polarization and waveform and applied to the corresponding images.

SA0610 VHR (St Gilles) Hh inc 40°			
Target/area	incidence	RCS / Sigma0 (dB)	Theo RCS (dB)
T8	38,54	17,17	17,4
T7	38,31	21,48	21,4
T6	38,43	24,24	24,4
T4	38,66	31,4	31,4
Flat water 1	36,12	-16,1	
Flat water 2	40,44	-20,08	
shadow	38,66	-18,64	

Table 4 : local incidence angle, measured and theoretical radar cross section for the corner reflectors and sigma0 value for the darkest image area.

2.2.2. SA0611, VHR, Vv polarization, incidence angle of 40°

Figure 11 : corner reflector area for SA611

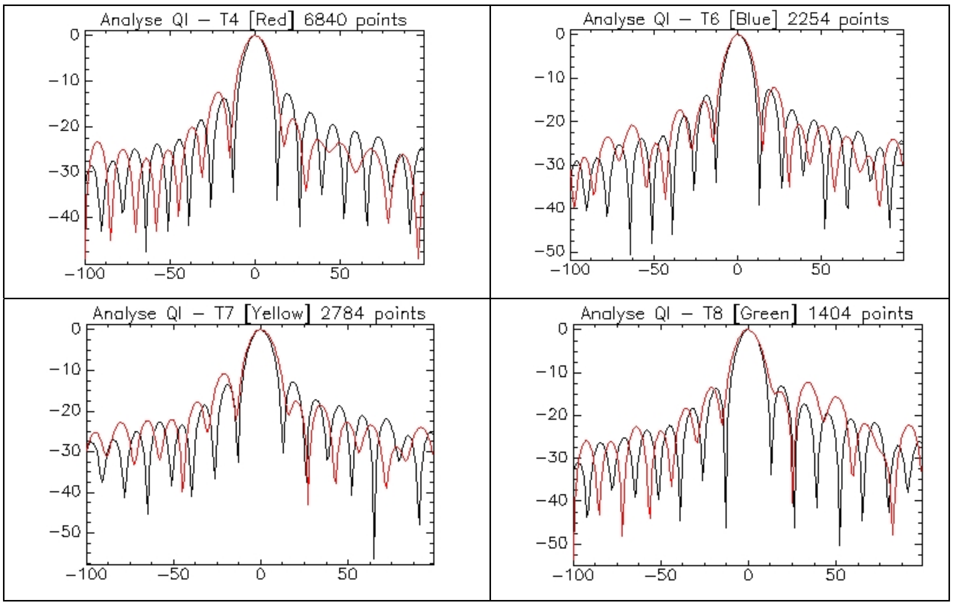

Figure 12 : response of the different corner reflectors along slant range direction in black and azimuth direction in red. Abscise is over-sampled Pixel (by 8).

SA0611 VHR (St Gilles) Vv inc 40°			
Target/area	incidence	RCS / Sigma0 (dB)	Theo RCS (dB)
T8	38,61	16,87	17,4
T7	38,37	21,61	21,4
T6	38,49	24,46	24,4
T4	38,73	31,13	31,4
Flat water 1	36,56	-15,59	
Flat water 2	40,67	-18,65	
dark area	38,62	-17,63	

Table 5 : local incidence angle, measured and theoretical radar cross section for the corner reflectors and sigma0 value for the darkest image area.

2.2.3. SA0602, VHR, Hh polarization, incidence angle of 40°

Figure 13 : corner reflector area for SA602

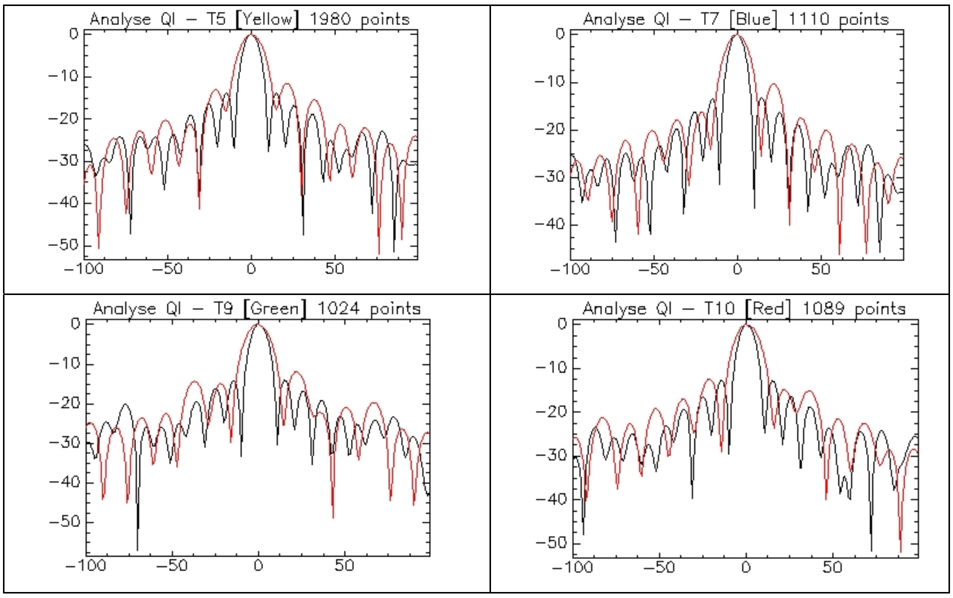

Figure 14 : response of the different corner reflectors along slant range in black and azimuth in red. Abscise is over-sampled Pixel (by 8).

SA0602 (Port la nouvelle) Hh inc 40°			
Target/area	incidence	RCS / Sigma0 (dB)	Theo RCS (dB)
T10	37,7	10,35	11,4
T9	37,94	14,12	14,4
T7	38,19	21,33	21,4
T5	38,45	27,59	27,4
flat sea	38,16	-21,56	

Table 6 : local incidence angle, measured and theoretical radar cross section for the corner reflectors and sigma0 value for the darkest image area.

2.2.4. SA0603, HR, Hh polarization, incidence angle of 40°

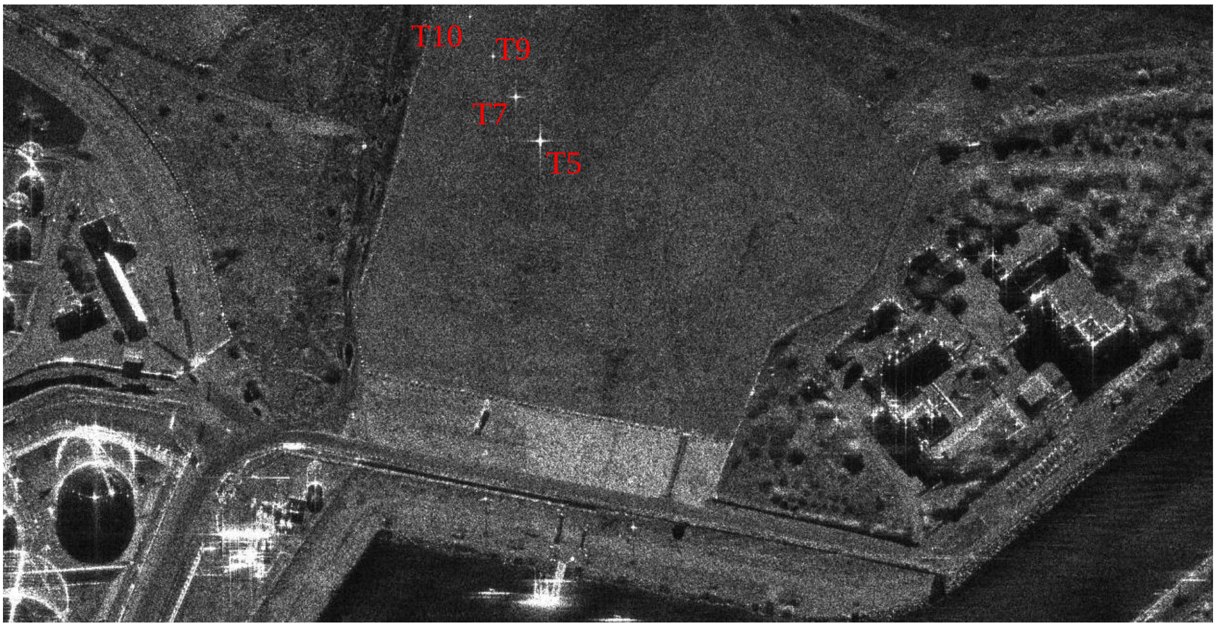

Figure 15 : corner reflector area for SA603

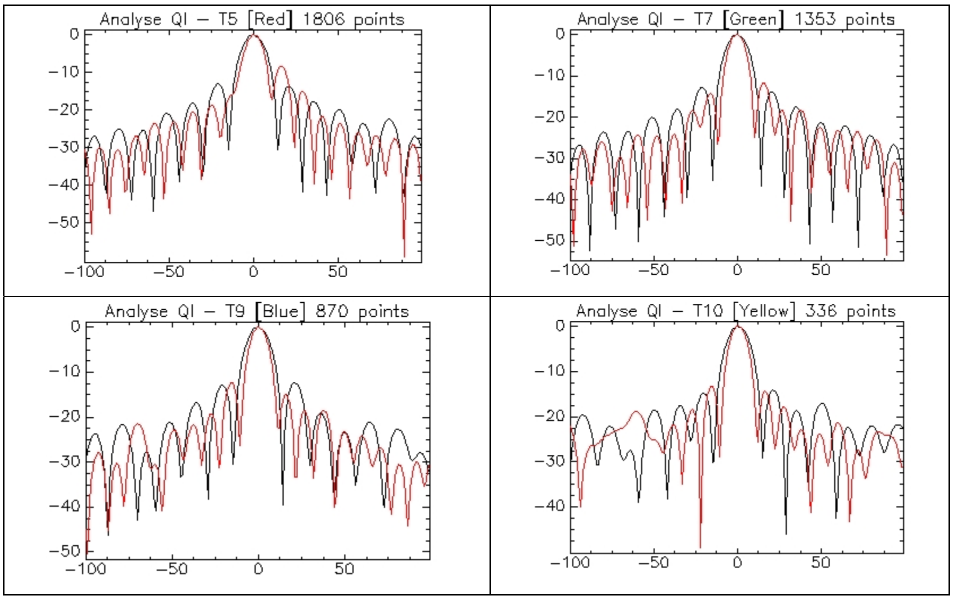

Figure 16 : response of the different corner reflectors along slant range in black and azimuth in red. Abscise is over-sampled Pixel (by 8).

SA0603 HR (Port la nouvelle) Hh inc 40°			
Target/area	incidence	RCS / Sigma0 (dB)	Theo RCS (dB)
T10	36,93	10,34	11,4
T9	37,18	14,72	14,4
T7	37,43	21,4	21,4
T5	37,69	27,47	27,4
Sand	38,15	-19,74	

Table 7 : local incidence angle, measured and theoretical radar cross section for the corner reflectors and sigma0 value for the darkest image area.

2.2.5. SA0605, VHR, Hh polarization, incidence angle of 60°

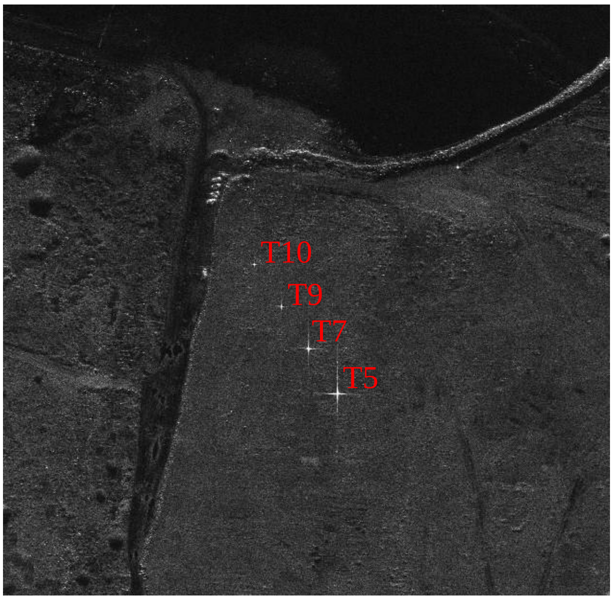

Figure 17 : corner reflector area for SA605

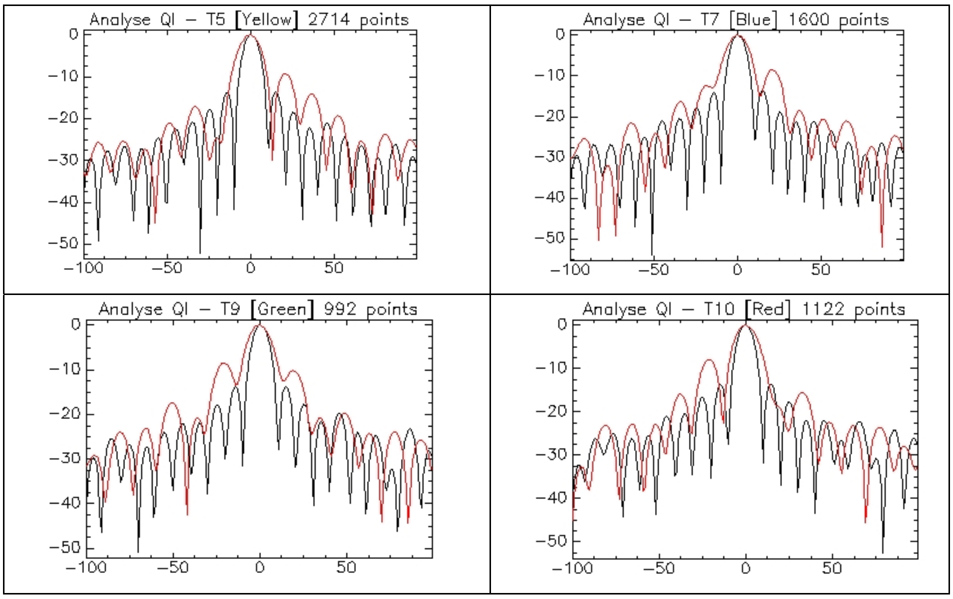

Figure 18 : response of the different corner reflectors along slant range in black and azimuth in red. Abscise is over-sampled Pixel (by 8).

SA0605 VHR (Port la nouvelle) Hh inc 60°			
Target/area	incidence	RCS / Sigma0 (dB)	Theo RCS (dB)
T10	58,22	11,16	11,4
T9	58,39	14,07	14,4
T7	58,55	21,21	21,4
T5	58,73	27,42	27,4
flat water	57,47	-20,87	

Table 8 : local incidence angle, measured and theoretical radar cross section for the corner reflectors and sigma0 value for the darkest image area.

2.2.6. Summary of the calibration performance

Based on the corner reflector analysis, we can conclude that the calibration accuracy is within the -0.4, 0.4 dB if we exclude the T10 reflector which is a little small (size 12.5 cm) to be reliable and could be mis-oriented (difficulty to orient a very small reflector)

The NE_Sigma0 is estimated to be better than the following values

image	Darkest area Sigma0	Bandwidth	incidence angle
SA0602	-21,56	1,22 GHz	40°
SA0603	-19,74	620 MHz	40°
SA0605	-20,87	1,22 GHz	60°
SA0610	-20,08	1,22 GHz	40°
SA0611	-18,65	1,22 GHz	40°

Table 9 : Summary of the darkest area Sigma0 for the available images.

2.3.Image analysis

In this paragraph the sigma0, or radar cross section (RCS), are analyzed for numerous regions of interest. Different kinds of areas are selected: agricultural field, town, industrial area, sea, swamp and river. The images below present the Region of Interested (ROI) from Figure 19 to Figure 23. The numbers in red in the images identify the ROIs for the analysis. The numbers in yellow in the images (Pr1 to Pr10) correspond to profiles of Sigma0 which are given in Figures 36 to 38.
We first present the histogram of RCS for town and industrial areas and the associated mean and standard deviation values in the tables of §4.1. Then, Sigma0 for natural ROIs are presented in the tables from §4.2 to §4.8 associated to each area type. Additionally, mean profiles are plotted for the sea showing the variation level due to different states of the sea (calm or rough).

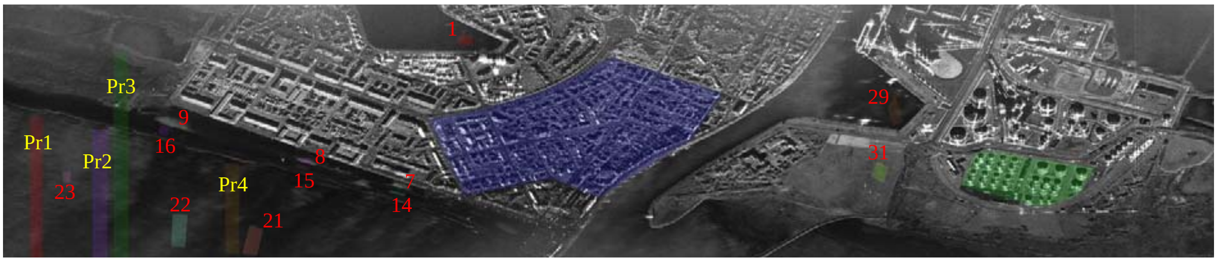

Figure 19 : SA0602 and the associated ROIs

Figure 20 : SA0603 and the associated ROIs

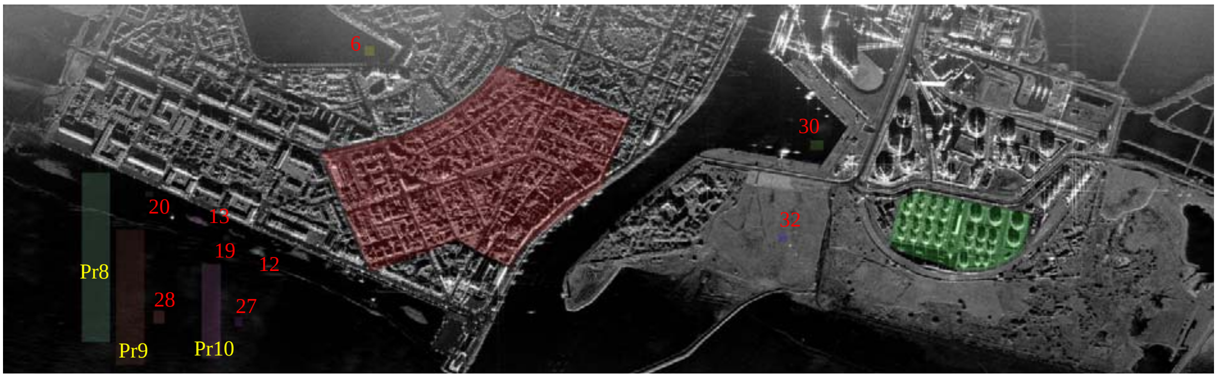

Figure 21 : SA0605 and the associated ROIs

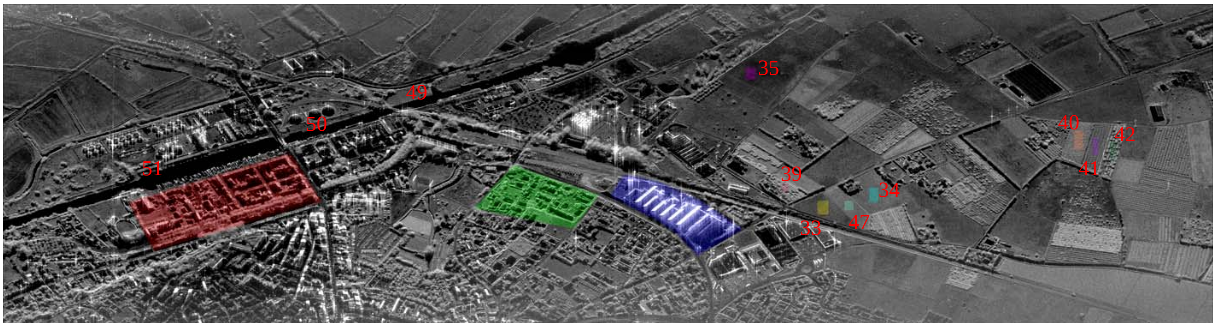

Figure 22 : SA0610 and the associated ROIs

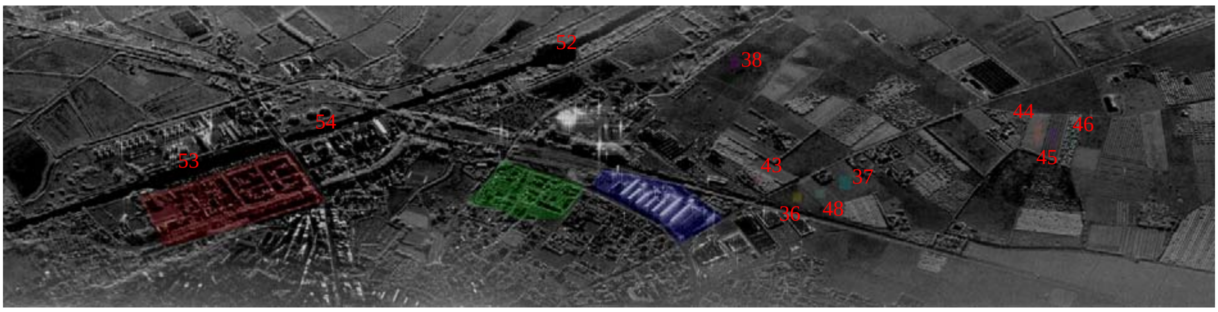

Figure 23 : SA0611 and the associated ROIs

2.3.1. Town and industrial areas

The values are presented in radar cross section (RCS) in linear form or in dBm2. One can easily transform a RCS to sigma0 values with the following formula:

$$\sigma_0\,[dBm^2/m^2] = RCS\,[dBm^2] - 10\log_{10}(S_r/\sin\theta)[dBm^2] = RCS - AdB$$

Where Sr is the surface of resolution (0.89 resolution_distance*resolution_azimuth) and q is the incidence angle. AdB is then the normalising surface.

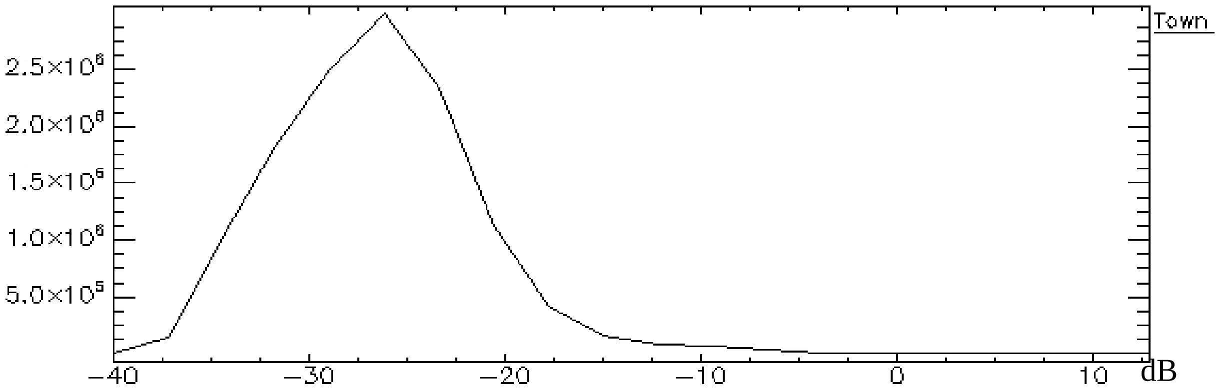

Figure 24 : RCS town histogram from image SA0602 (multi look 5x5, => ENL=11.3) Fig 19 blue ROI

SA0602	Single look		5x5 Multi look, ENL=11.3	
town	RCS mean	RCS std	RCS mean	RCS std
linear	0,013	0.300	0,013	0.133
dB	-18.95		-18.95	

Table 10 : associated mean and max values from SA0602 (single and 5x5 multi-look), Fig 19 blue ROI-AdB=-14.4 dB

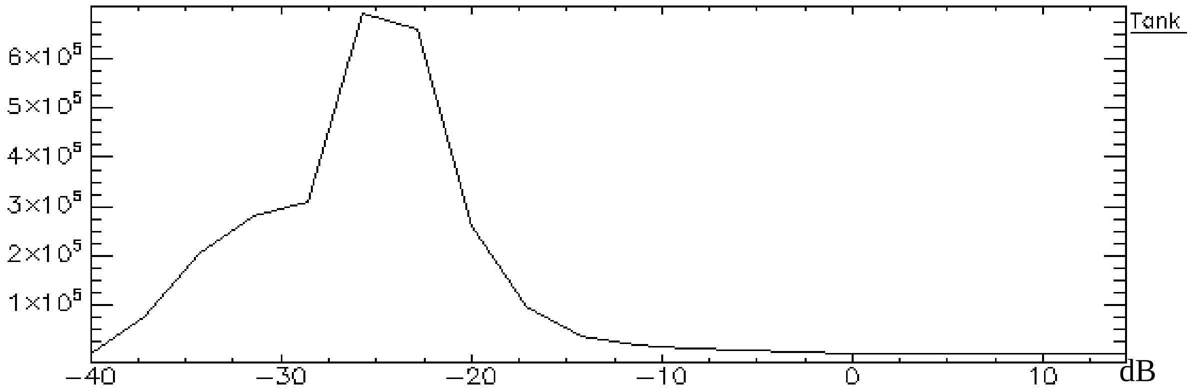

Figure 25 : RCS tank area histogram from image SA0602 (multi look 5x5, ENL=11.3) Fig 19 green

SA0602	Single look		5x5 Multi look, ENL=11.3	
tank	RCS mean	RCS std	RCS mean	RCS std
linear	0.028	0.884	0.028	0.425
dB	-15.58		-15.58	

Table 11 : associated mean and max values from SA0602 (single and 5x5 multi-look), Fig 19 green ROI, AdB= -14.2 dB

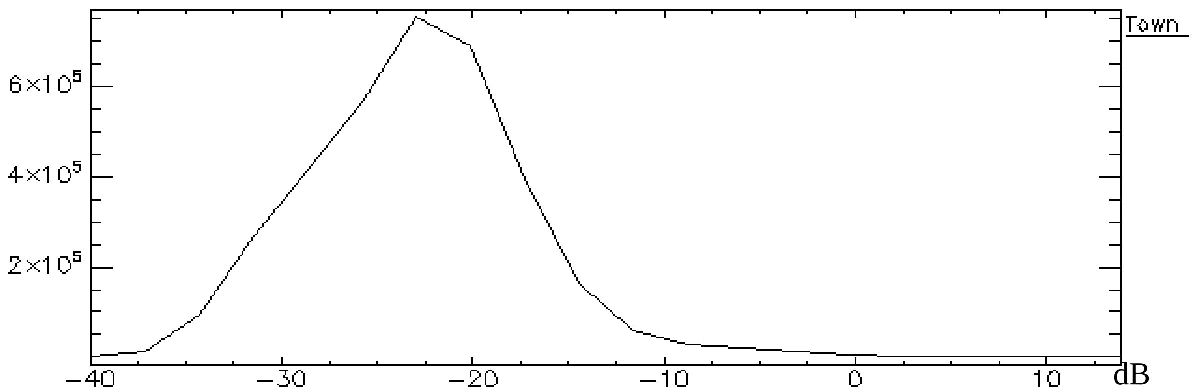

Figure 26 : RCS town histogram from image SA0603 (multi look 5x5, ENL=11.4) Fig 20 red ROI

SA0603	Single look		5x5 Multi look, ENL=11.4	
town	RCS mean	RCS std	RCS mean	RCS std
linear	0.056	0.802	0.056	0.339
dB	-12.48		-12.48	

Table 12 : associated mean and max values from SA0603 (single and 5x5 multi-look), Fig 20 red ROI , AdB= -9.7 dB

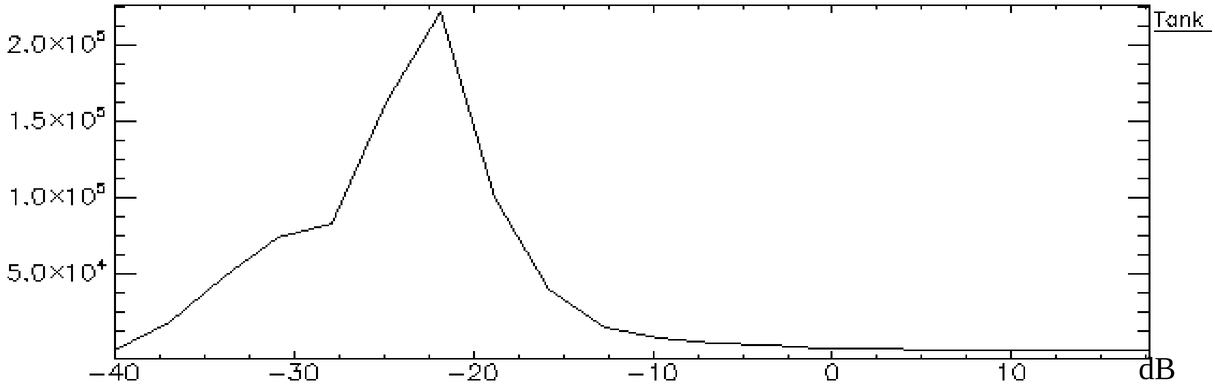

Figure 27 : RCS tank area histogram from image SA0603 (multi look 5x5, ENL=11.4) Fig 20 green ROI

SA0603	Single look		5x5 Multi look, ENL=11.4	
tank	RCS mean	RCS std	RCS mean	RCS std
linear	0.102	2.871	0.102	1.286
dB	-9.91		-9.91	

Table 13 : associated mean and max values from SA0603 (single and 5x5 multi-look), Fig 20 green ROI, AdB= -9.5 dB

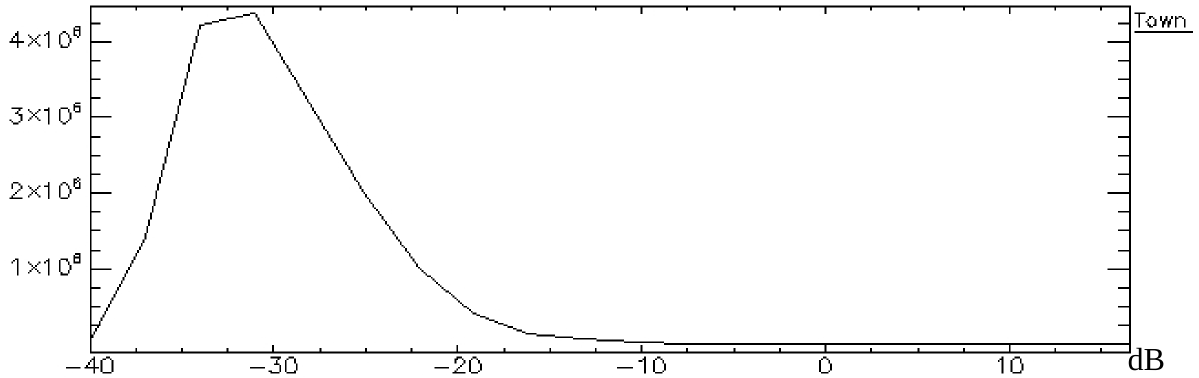

Figure 28 : RCS town histogram from image SA0605 (multi look 5x5, ENL=11.3) Fig 21 red ROI

SA0605	Single look		5x5 Multi look, ENL=11.3	
town	RCS mean	RCS std	RCS mean	RCS std
linear	0.007	0.447	0.007	0.179
dB	-21.82		-21.82	

Table 14 : associated mean and max values from SA0605 (single and 5x5 multi-look), Fig 21 red ROI, , AdB= -16.0 dB

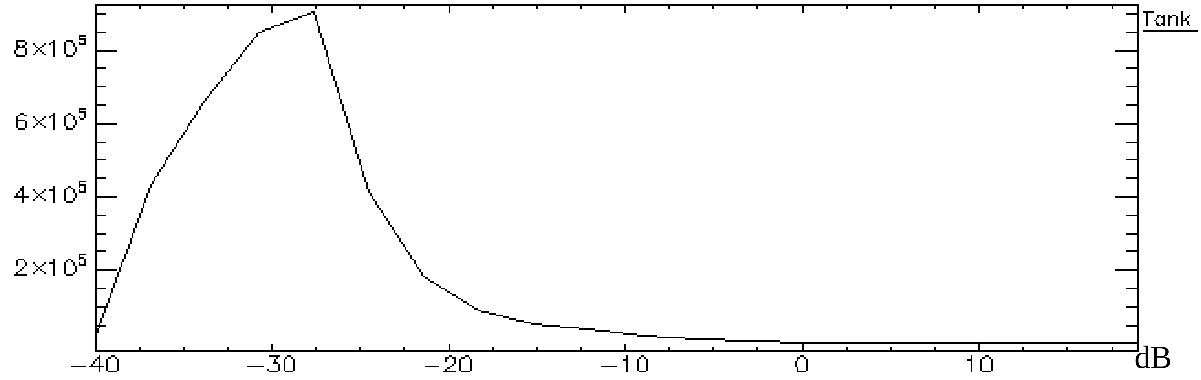

Figure 29 : RCS tank area histogram from image SA0605 (multi look 5x5, ENL=11.3) Fig 21 green ROI

SA0605	Single look		5x5 Multi look, ENL=11.3	
tank	RCS mean	RCS std	RCS mean	RCS std
linear	0.022	1.650	0.022	0.762
dB	-16.57		-16.57	

Table 15 : associated mean and max values from SA0605 (single and 5x5 multi-look), Fig 21 green ROI, ,

AdB= -15.9 dB

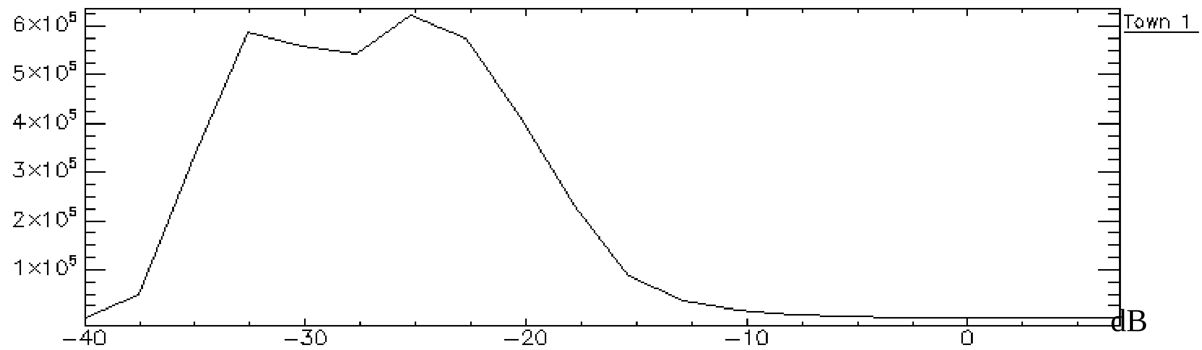

Figure 30 : RCS town histogram from image SA0610 (multi look 5x5, ENL=11.3) Fig 22 red ROI

SA0610	Single look		5x5 Multi look, ENL=11.3	
town 1	RCS mean	RCS std	RCS mean	RCS std
linear	0.012	0.150	0.012	0.064
dB	-19.24		-19.24	

Table 16 : associated mean and max values from SA0610 (single and 5x5 multi-look), Fig 22 red ROI, ,

AdB= -14.8 dB

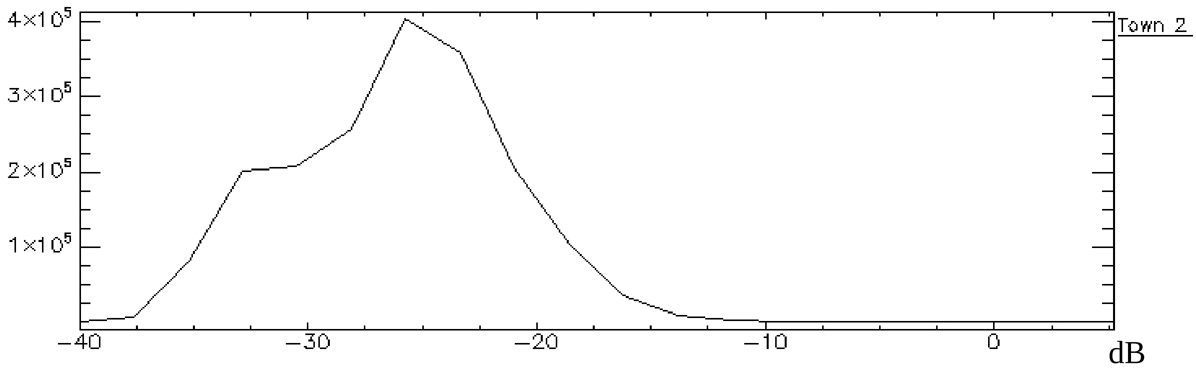

Figure 31 : RCS town histogram from image SA0610 (multi look 5x5, ENL=11.3) Fig 22 green ROI

SA0610	Single look		5x5 Multi look, ENL=11.3	
town 2	RCS mean	RCS std	RCS mean	RCS std
linear	0.011	0.105	0.011	0.051
dB	-19.56		-19.56	

Table 17 : associated mean and max values from SA0610 (single and 5x5 multi-look), Fig 22 green ROI, ,

AdB= -14.8dB

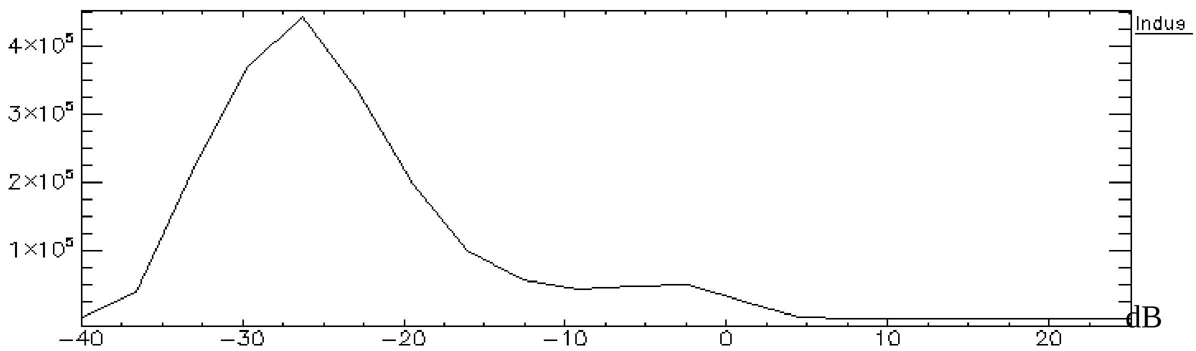

Figure 32 : RCS industrial area histogram from image SA0610 (multi look 5x5, ENL=11.3) Fig 22 blue ROI

SA0610	Single look		5x5 Multi look, ENL=11.3	
Industry	RCS mean	RCS std	RCS mean	RCS std
linear	0.269318	9.707	0.269	3.977
dB	-5.70		-5.70	

Table 18 : associated mean and max values from SA0610 (single and 5x5 multi-look), Fig 22 blue ROI, ,

AdB=-14.8dB

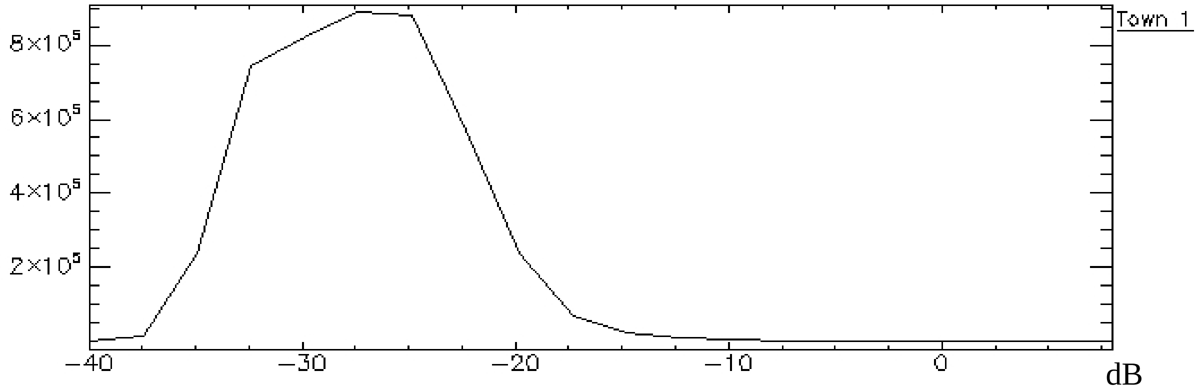

Figure 33 : RCS town histogram from image SA0611 (multi look 5x5, ENL=8.53) Fig 23 red ROI

SA0611	Single look		5x5 Multi look, ENL=8.53	
town 1	RCS mean	RCS std	RCS mean	RCS std
linear	0.0068	0.079	0.0068	0.037
dB	-21.66		-21.66	

Table 19 : associated mean and max values from SA0611 (single and 5x5 multi-look), Fig 23 red ROI, , AdB=-13.8 dB

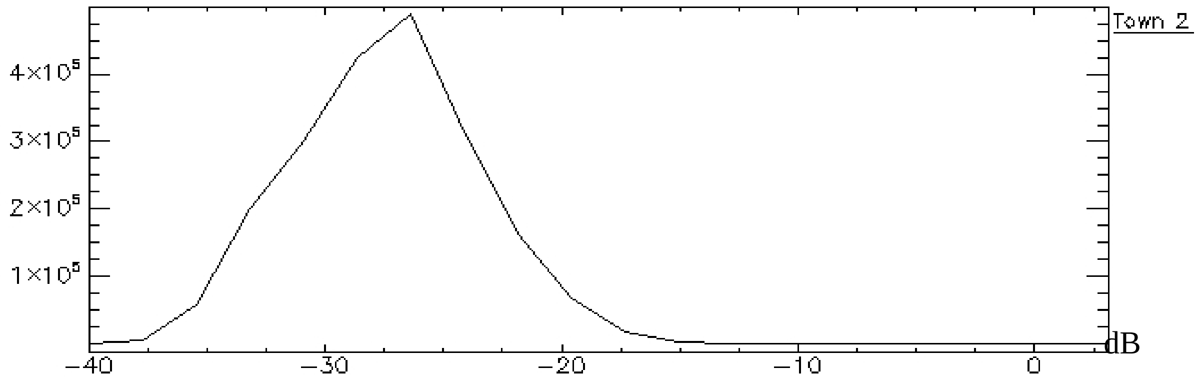

Figure 34 : RCS town histogram from image SA0611 (multi look 5x5, ENL=8.53) , Fig 23 green ROI

SA0611	Single look		5x5 Multi look, ENL=8.53	
town 2	RCS mean	RCS std	RCS mean	RCS std
linear	0.0076	0.047	0.0076	0.025
dB	-21.19		-21.19	

Table 20 : associated mean and max values from SA0611 (single and 5x5 multi-look) , Fig 23 green ROI, AdB=-13.8 dB

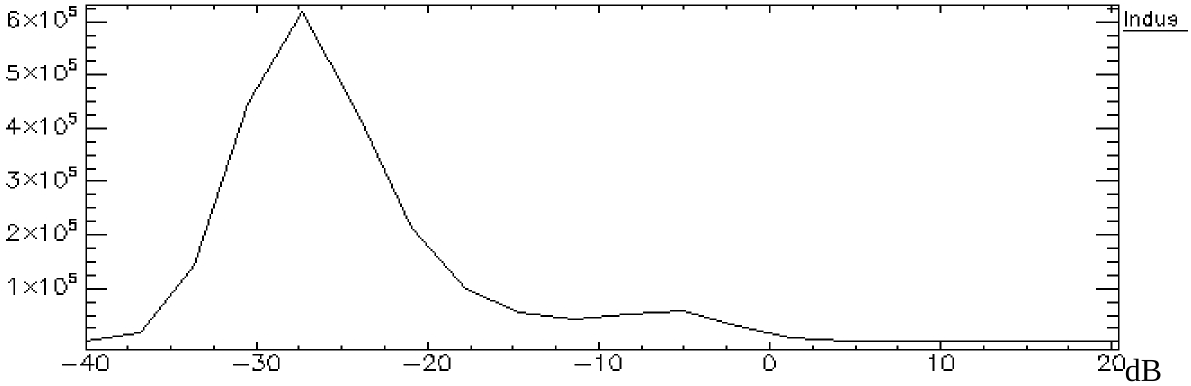

Figure 35 : RCS industry histogram from image SA0611 (multi look 5x5, ENL=8.53) , Fig 23 blue ROI

SA0611	Single look		5x5 Multi look, ENL=8.53	
Industry	RCS mean	RCS std	RCS mean	RCS std
linear	0.112	2.935	0.112	1.279
dB	-9.52		-9.52	

Table 21 : associated mean and max values from SA0611 (single and 5x5 multi-look) , Fig 23 blue ROI, AdB=-13.8 dB

2.3.2. Swamp

The last two colums are corresponding to the mean of the sigma0 power and the standard deviation of the sigma0 power on the SLC image.

ROI N°	type of area	image	Polarization	incidence angle	Sigma0 (dB)	Sigma0 (lin)	Sigma0 Std (lin)
1	Swamp	SA0602	Hh	43,7°	-11,72	0,06729767	0,07
2	swamp	SA0603	Hh	40,60°	-9,81	0,10447202	0,07
3	swamp	SA0603	Hh	38,46°	-10,32	0,09289664	0,10
4	swamp	SA0603	Hh	41,84°	-10,13	0,097051	0,11
5	swamp	SA0603	Hh	40,61°	-9,06	0,12416523	0,13
6	swamp	SA0605	Hh	62,05°	-10,68	0,08550667	0,09

2.3.3. Sand

ROI N°	type of area	image	Polarization	incidence angle	Sigma0 (dB)	Sigma0 (lin)	Sigma0 Std (lin)
7	dry sand	SA0602	Hh	38,45°	-8,57	0,13899526	0,17
8	dry sand	SA0602	Hh	39,42°	-7,58	0,17458222	0,21
9	dry sand	SA0602	Hh	40,95°	-7,3	0,18620871	0,23
10	dry sand	SA0603	Hh	40,04°	-7,65	0,17179084	0,20
11	dry sand	SA0603	Hh	37,67°	-8,06	0,15631476	0,17
12	dry sand	SA0605	Hh	58,60°	-11,01	0,07925013	0,10
13	dry sand	SA0605	Hh	59,18°	-12,16	0,0608135	0,08

ROI N°	type of area	image	Polarization	incidence angle	Sigma0 (dB)	Sigma0 (lin)	Sigma0 Std (lin)
14	wet sand	SA0602	Hh	38,14°	-19,96	0,01009253	0,01
15	wet sand	SA0602	Hh	39,19°	-19	0,01258925	0,01
16	wet sand	SA0602	Hh	40,61°	-18,85	0,01303167	0,01
17	wet sand	SA0603	Hh	39,59°	-21,68	0,00679204	0,01
18	wet land	SA0603	Hh	39,34°	-18,02	0,01577611	0,02
19	wet land	SA0605	Hh	58,87°	-20,32	0,00928966	0,01
20	wet land	SA0605	Hh	59,68°	-19,17	0,01210598	0,01

2.3.4. Sea

ROI N°	type of area	image	Polarization	incidence angle	Sigma0 (dB)	Sigma0 (lin)	Sigma0 Std (lin)
21	sea	SA0602	Hh	36°	-17,43	0,01807174	0,02
22	sea	SA0602	Hh	36,51°	-12,92	0,0510505	0,05
23	sea	SA0602	Hh	39,01°	-10,77	0,08375293	0,09
24	sea	SA0603	Hh	38,34°	-10,53	0,08851156	0,10
25	sea	SA0603	Hh	39,96°	-9,68	0,10764652	0,11
26	sea	SA0603	Hh	38,12°	-9,01	0,125603	0,13
27	sea	SA0605	Hh	57,18°	-17,18	0,01914256	0,02
28	sea	SA0605	Hh	57,28°	-19,69	0,01073989	0,11

ROI N°	type of area	image	Polarization	incidence angle	Sigma0 (dB)	Sigma0 (lin)	Sigma0 Std (lin)
29	sea port	SA0602	Hh	41,19°	-15,42	0,02870781	0,03
30	sea port	SA0605	Hh	60,54°	-17,38	0,018281	0,02

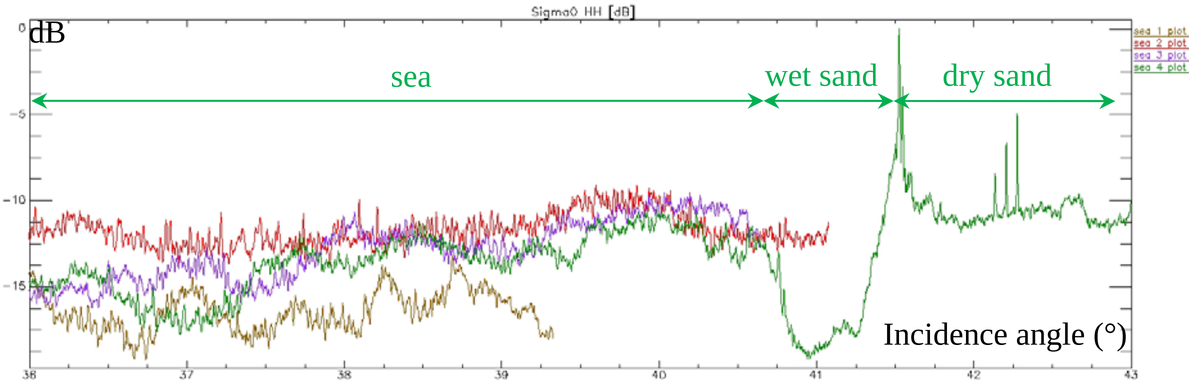

Figure 36 : sea mean sigma0 profile from image SA0602

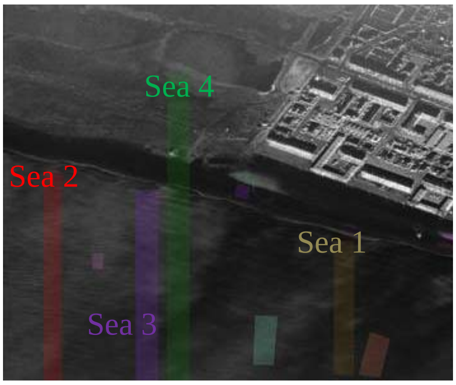

Figure 36a: sea ROI corresponding to fig 36 profiles

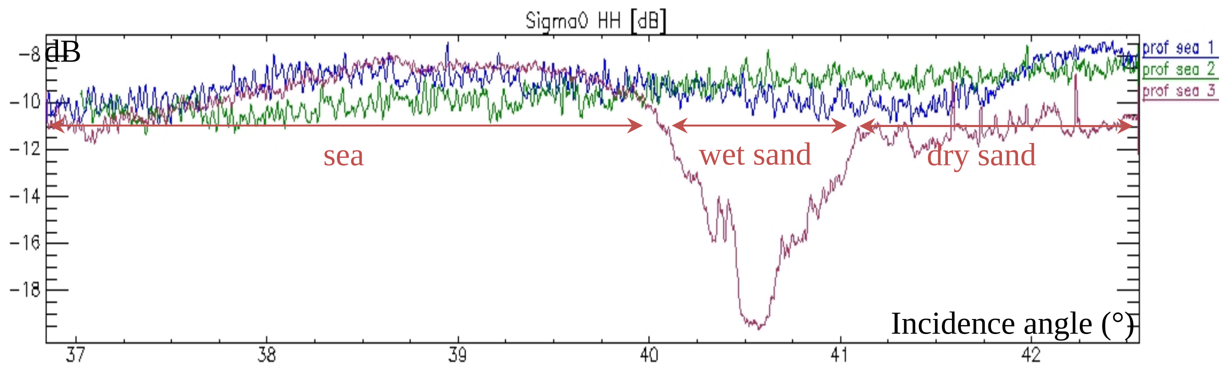

Figure 37 : sea mean sigma0 profile from image SA0603

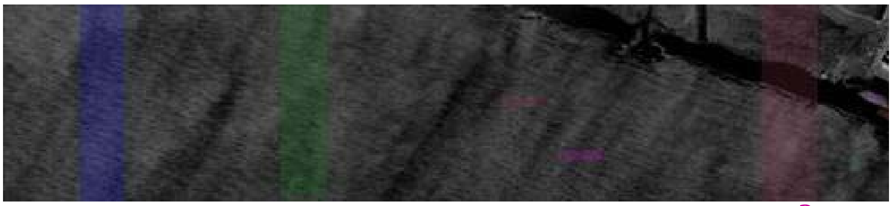

Figure 37a: sea ROI corresponding to fig 37 profiles

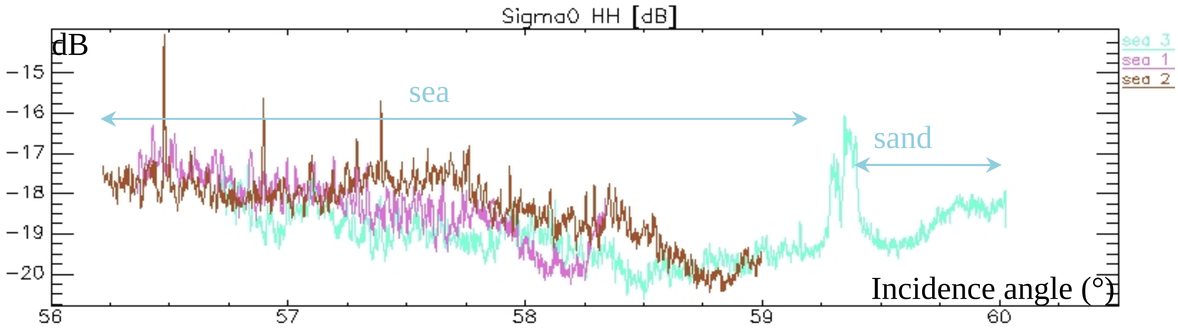

Figure 38: sea mean sigma0 profile from image SA0605

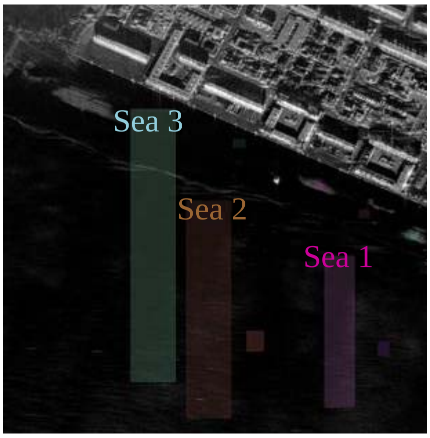

Figure 38a: sea ROI corresponding to fig 38 profiles

2.3.5. Meadow

ROI N°	type of area	image	Polarization	incidence angle	Sigma0 (dB)	Sigma0 (lin)	Sigma0 Std (lin)
31	Corner reflector area	SA0602	Hh	39,02°	-8,14	0,1534617	0,17
32	Corner reflector area	SA0605	Hh	58,87°	-10,36	0,09204496	0,10

ROI N°	type of area	image	Polarization	incidence angle	Sigma0 (dB)	Sigma0 (lin)	Sigma0 Std (lin)
33	meadow	SA0610	Hh	41,83°	-7,86	0,005448	0,18
34	meadow	SA0610	Hh	41,42°	-6,09	0,008252	0,26
35	meadow	SA0610	Hh	36,98°	-11,62	0,002538	0,07
36	meadow	SA0611	Vv	41,96°	-9,2	0,00504	0,13
37	meadow	SA0611	Vv	41,46°	-8,2	0,006413	0,16
38	meadow	SA0611	Vv	36,86°	-10,51	0,004154	0,10

2.3.6. Orchard

ROI N°	type of area	image	Polarization	incidence angle	Sigma0 (dB)	Sigma0 (lin)	Sigma0 Std (lin)
39	orchard	SA0610	Hh	41,18°	-2,68	0,53951062	0,71
40	orchard	SA0610	Hh	39,92°	-4,96	0,31915379	0,50
41	orchard	SA0610	Hh	39,77°	-6,33	0,23280913	0,30
42	orchard	SA0610	Hh	39,53°	-4,83	0,32885163	0,44
43	orchard	SA0611	Vv	41,29°	-4,07	0,39174188	0,51
44	orchard	SA0611	Vv	39,81°	-6,1	0,24547089	0,40
45	orchard	SA0611	Vv	39,77°	-7,5	0,17782794	0,24
46	orchard	SA0611	Vv	39,65°	-5,53	0,27989813	0,35

2.3.7. Vineyard

ROI N°	type of area	image	Polarization	incidence angle	Sigma0 (dB)	Sigma0 (lin)	Sigma0 Std (lin)
47	vineyard	SA0610	Hh	41,77°	-5	0,31622777	0,46
48	vineyard	SA0611	Vv	41,83°	-6,77	0,21037784	0,35

2.3.8. River

ROI N°	type of area	image	Polarization	incidence angle	Sigma0 (dB)	Sigma0 (lin)	Sigma0 Std (lin)
49	water	SA0610	Hh	38,15°	-18,96	0,01270574	0,01
50	water	SA0610	Hh	40,96°	-20,35	0,00922571	0,01
51	water	SA0610	Hh	39,19°	-19	0,01258925	0,01
52	water	SA0611	Vv	36,58°	-15,49	0,0282488	0,03
53	water	SA0611	Vv	41,07°	-17,93	0,01610646	0,02
54	water	SA0611	Vv	39,45°	-18,78	0,01324342	0,01

2.3.9. Summary of the analysis

The analysis of the Sigma0 for different kinds of ROI shows an interesting contrast.

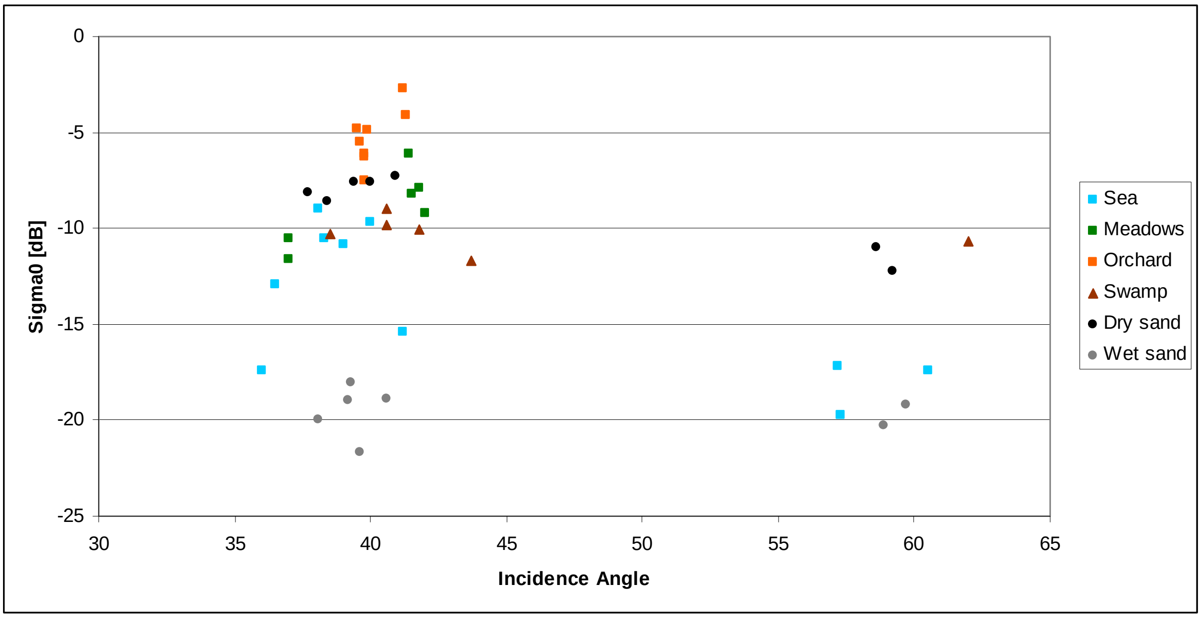

Over the sea: The observed variation in reflectivity over the different sea areas can be extremely high (from -9 to -19 dB). The analysed images were acquired on the same date, with the same route. The variation is therefore not linked to different weather conditions nor to different azimuth angle. It is linked to the local variation of sea state, where calm streaks of water are found due to local conditions. The Sigma0 values for the river varies from -17 to -20 dB similarly to calm water. The relatively high values measured for the sea inside the harbour compared to the open sea are certainly resulting from sidelobes arising from the structures around the water.

For land targets, the urban areas are characterised by very bright point targets (associated with a high radar cross section) set on a low background (low sigma0)
The orchard areas have a high sigma0 value around -5dB. The meadows have slightly lower sigma0 values. This could be linked to a saturation of the roughness effect at these high frequencies. The radar backscatters are yet lower for the swamps (about 3dB).
The dry sand exhibits a decrease of backscatter as a function of incidence. This is indeed a smooth surface from which such behaviour is expected. The wet sand has a very weak signal, maybe close to the noise level in the data.

3. DRIVE-BUSARD dedicated Ka Band campaign

3.1. General description

Figure 38 : BUSARD in flight.

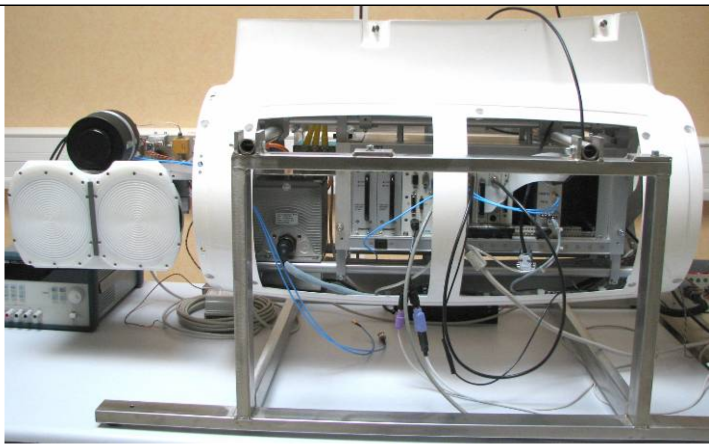

Figure 39 : The Ka radar, DRIVE.

ONERA, the French space lab, acquired in December 2004 a motor-glider STEMME S10-VT (Figure 38) modified in order to be used as a test bench for compact, light and low energy UAV payloads. The first instrument to be designed and tested was the radar system DRIVE operating at Ka band.

DRIVE is a 35 GHz SAR (Figure 39) based on an IFMCW (Interrupted Frequency Modulation Continuous Wave) mode. This type of mode is characterised by two antennas operating simultaneously one in transmission and the other in reception. The main advantage of such a mode is a low peak power requirement as the chirp waveform is very long compared to a more classical mode.

The DRIVE radar has an adjustable mount for the antenna, with a selectable boresight angle ranging from 0° incidence (nadir looking) to 90° incidence (horizontal – grazing) in steps of 5°. This adjustment has to be performed on the ground; therefore one flight is acquired in a single configuration.
For the SAR imaging mode, rectangular horn antennas are used and the current setting is Vv polarisation.

3.1.1. Campaign wave form and geometry

In order to cover the incidence angle range from 20° to 50°, we have selected to fly with two different configurations:

- One with a boresight incidence angle of 30°
- The other with a boresight incidence angle of 40°

By shifting the flight track by about 80m, both configurations cover the same swath, resulting in a more direct way of analysing the backscattering behaviour as a function of incidence. This is illustrated in Figure 40.

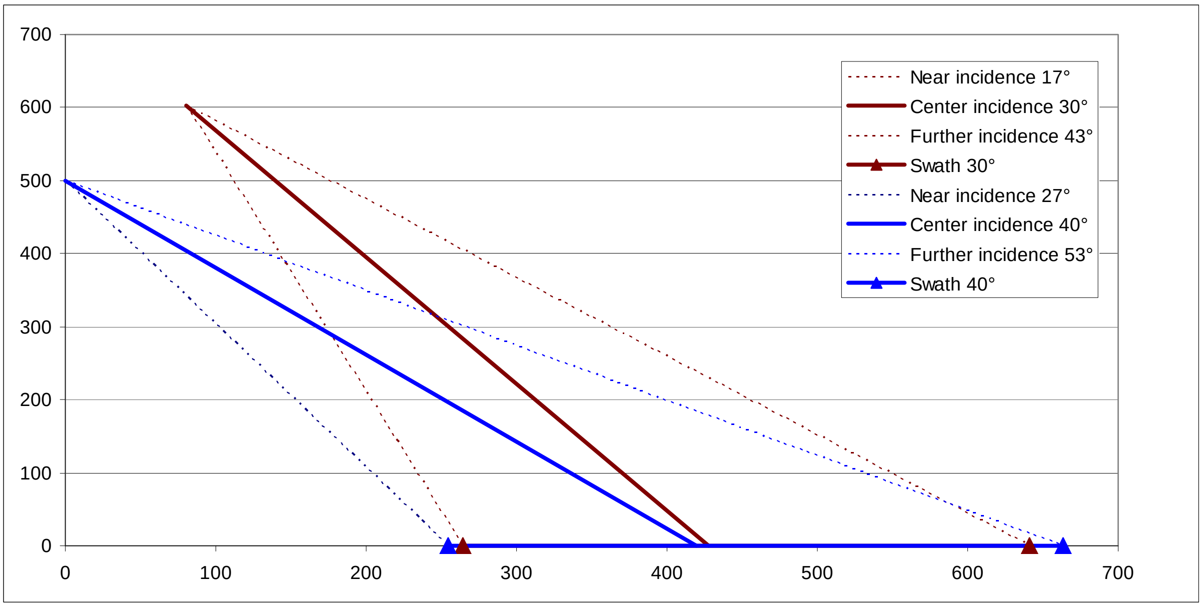

Figure 40 : The two acquisition geometries with boresight incidence angles of 30° and 40°.

Table 22 **: Wave form characteristics**

Band	Centre Frequency[GHz]	Bandwidth [MHz]	Antenna	PRF	Tx Power	Polarimetry
Ka	35	400 MHz	Horns 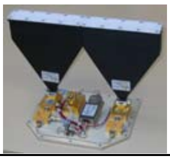	2000 Hz	2.5 W	Vv

The selected wave form is 400MHz, allowing a slant range resolution of $\delta_s = \frac{0.89c}{2B} = 0.33m$ when using a rectangular weighting function. This value projects into a ground resolution at 45° incidence of 0.47 m.

3.2.Description of the dataset

The KaSAR campaign has been conducted in July and September 2012 in Southern France with the ONERA airborne system DRIVE on the BUSARD platform. The main objective of this campaign was to collect data at Ka Band over natural areas. . The acquisitions took place in the South of France over St Gilles, Piemanson, Rhone River (south of Arles) and Fos-sur-

Mer gulf, two with an incidence angle of 30° and one with an incidence angle of 40°. Figure 41 and Figure 42 localise these areas.

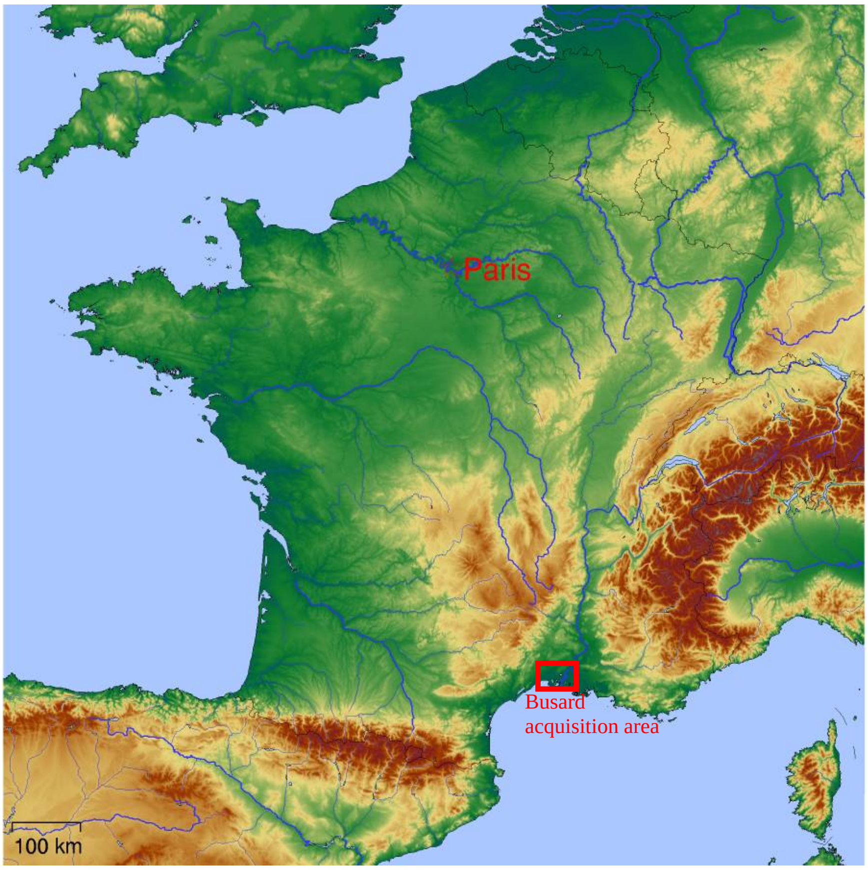

Figure 41 : location of imaged area.

Figure 42 : ©GoogleMap image of the Drive-Busard acquisition locations in South of France (zoom of Figure 41).

The imaged scenes are composed of the coastal area of Piemanson, of St Gilles agricultural landscape, of the Rhone river area and of open sea in the Fos-sur-Mer gulf. The data were acquired in high resolution, 400 MHz bandwidth, with a central frequency of 35 GHz. Table 23 summarizes the main system parameters, for DRIVE-BUSARD, used during the acquisition campaign.

Parameters	HR
Central frequency	35 GHz
wave form	FMCW
PRF	2000 Hz
Sampling rate	20 MHz
Bandwidth	400 MHz

Table 23 : summary of the system parameters

Several corner reflectors were deployed in St Gilles and Piemanson to achieve the calibration of the data.
The delivered data and their principal characteristics are listed in Table 24. The flight altitude was lowered with respect of the validation flight in order to counter the interferences from system and the in-flight photos have the same incidence angle as the radar but cover a slightly

smaller area because the camera zoom was left adjusted for the higher flight track of the validation flight.

	Polarization	Resolution	incidence angle	Imaged area	Altitude above ground	Acquisition date
KaSAR104	Vv	HR	30°	St Gilles	580m	11/07/2012
KaSAR204	Vv	HR	30°	St Gilles	626m	17/09/2012
KaSAR304	Vv	HR	40°	St Gilles	493m	18/09/2012
KaSAR107	Vv	HR	30°	Piemanson	607m	11/07/2012
KaSAR208	Vv	HR	30°	Piemanson	629m	17/09/2012
KaSAR308	Vv	HR	40°	Piemanson	491m	18/09/2012
KaSAR103	Vv	HR	30°	Rhone	571m	11/07/2012
KaSAR311	Vv	HR	40°	Fos-sur-Mer gulf	498m	18/09/2012

Table 24 : Ka band images acquired by Drive-Busard.

The weather during the flights was:

- RAMSES data acquired on June 3rd 2008: wind speed for Port la Nouvelle: 25km/h with gusts of wind at 45km/h.
- DRIVE-BUSARD data acquired on
  - July 11th: Wind speed: 25km/h with gusts up to 40km/h Significant wave height: 0.6m with max 1.2m
  - September 17tth: Wind speed: 7km/h with gusts of 13km/h
  - September 18th: Wind speed: 7km/h with gusts of 11km/h

The wave height information is not available over the area for the 17th and the 18th September. The water was smooth, with very little waves.

For all the delivered images the slant range resolution is 0.39m and the azimuth resolution is 0.35m. The pixel size is 0.25m along both axes.

There was no significant change in soil moisture of selected land targets from July to September.

Due to its light weight, BUSARD motor glider motions are very sensitive to the wind. Furthermore, the antenna has a very narrow azimuth beamwidth. A small squint angle will move the antenna pattern outside of the area of interest. We chose to process complete acquisitions (including areas for which the illumination is not optimum). A mask is provided together with the images in order to identify the portions of the images falling within the 3dB pattern (6dB round trip). The sigma0 values are reliable inside the mask area. The masks are included in the delivered data.

The antenna pattern is taken into account in the delivered dataset. However, we do not know the pattern well enough outside the 3dB beamwidth where we believe we are over-compensating its effect.
We present the delivered SLC images and the associated mask.

3.2.1. St Gilles agricultural landscape

3.2.1.1. KaSAR104, incidence angle of 30°

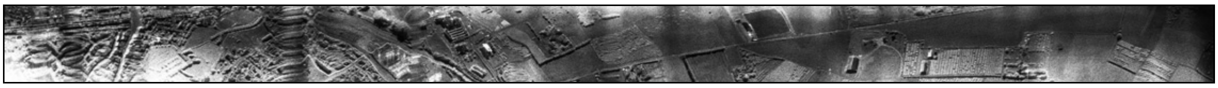

Figure 43 : magnitude image, image size 740x11827 pixels.

Figure 44 : mask from the antenna pattern

Figure 45 : mask applied on the magnitude image

3.2.1.2. KaSAR204, incidence angle of 30°

Figure 46 : magnitude image, image size 740x12145 pixels.

Figure 47 : mask from the antenna pattern

Figure 48 : mask applied on the magnitude image

3.2.1.3. KaSAR304, incidence angle of 40°

Figure 49 : magnitude image, image size 1100x8128 pixels.

Figure 50 : mask from the antenna pattern

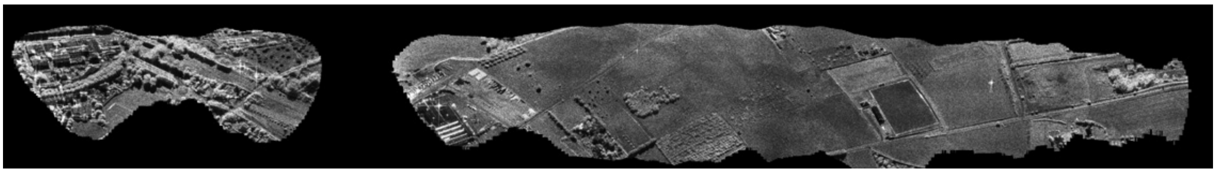

Figure 51 : mask applied on the magnitude image

3.2.2. Piemanson sea coast

3.2.2.1. KaSAR107, incidence angle of 30°

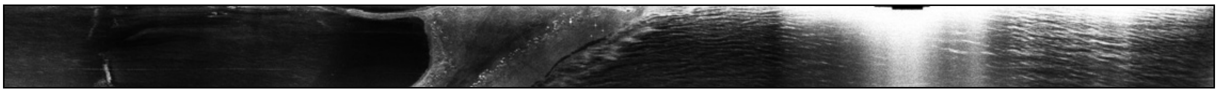

Figure 52 : magnitude image, image size 740x11069 pixels.

Figure 53 : mask from the antenna pattern

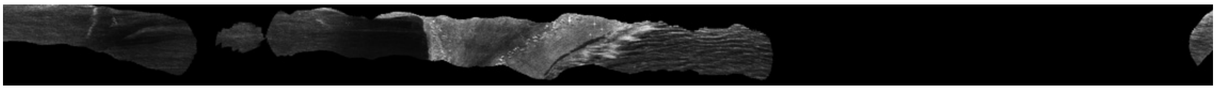

Figure 54 : mask applied on the magnitude image

3.2.2.1. KaSAR208, incidence angle of 30°

Figure 55 : magnitude image, image size 740x13130 pixels.

Figure 56 : mask from the antenna pattern

Figure 57 : mask applied on the magnitude image

3.2.2.2. KaSAR308, incidence angle of 40°

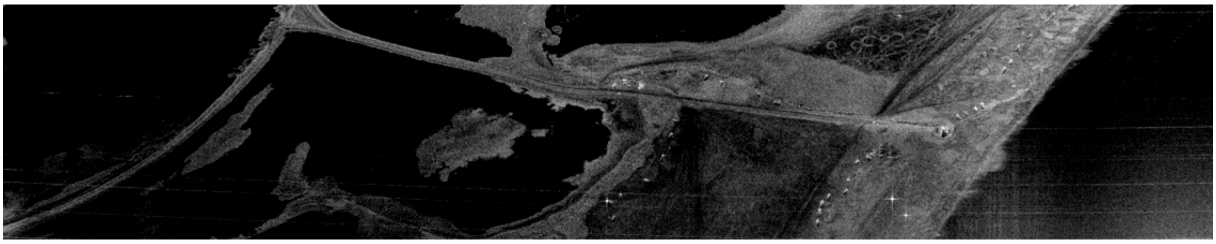

Figure 58 : magnitude image, image size 1100x5703 pixels.

Figure 59 : mask from the antenna pattern

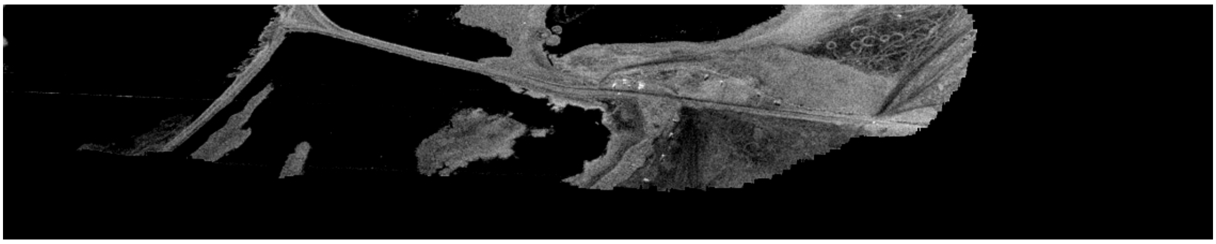

Figure 60 : mask applied on the magnitude image

3.2.3. Rhone area

3.2.3.1. KaSAR103, incidence angle of 30°

Figure 61 : magnitude image, image size 740x8004 pixels.

Figure 62 : mask from the antenna pattern

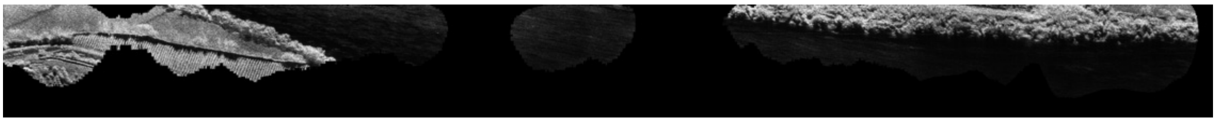

Figure 63 : mask applied on the magnitude image

3.2.4. Fos-sur-Mer gulf

3.2.4.1. KaSAR311, incidence angle of 40°

Figure 64 : magnitude image, image size 1100x7770 pixels.

Figure 65 : mask from the antenna pattern

Figure 66 : mask applied on the magnitude image

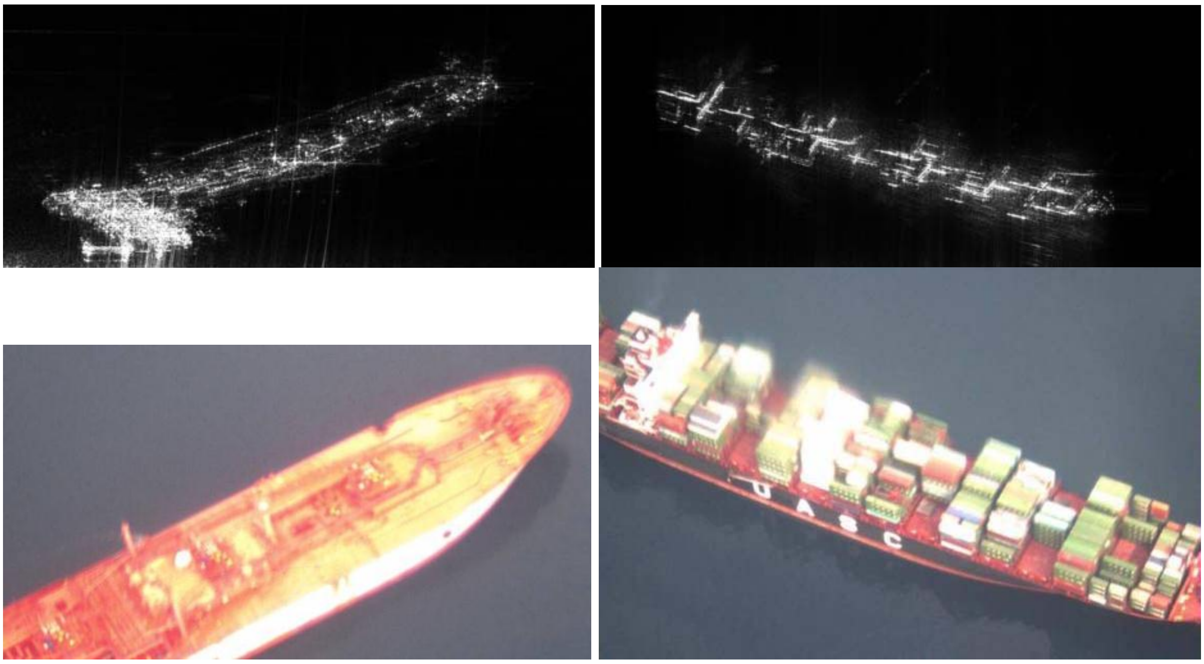

Figure 67 : zoom on the boats from magnitude image and the associated optical images acquired simultaneously by onboard camera.

3.3. Calibration analysis

The calibration process is based on the corner reflectors deployed during each flight (Figure 68, Figure 69). The same calibration key is applied on each image from the same flight, weighted by the variation of the electronic attenuation which could vary from pass-to-pass.

Figure 68 : set of Ka corner reflectors (left), corner reflectors deployed on Piemanson beach.

Figure 69 : corner reflectors deployed in St Gilles area (left) and in Rhone area (right).

The corner reflectors theoretical and measured values are presented Table 25 for the images used to calibrate the three flights. The responses of these reflectors are presented from Figure 70 to Figure 72.

Corner reflector	size (m)	Theo RCS (dB)	Measured RCS (dB)
KaSAR107 T5	0,264	27.37	27.72
KaSAR107 T7	0,222	21.4	21.75
KaSAR204 T5	0,264	27.42	27.42
KaSAR204 T7	0,222	21,4	20.08
KaSAR304 T5	0,264	27.43	27.43
KaSAR304 T7	0,222	21.4	21.69

Table 25 size and theoretical values (in dB) of the corner reflectors deployed for Drive-Busard KaSAR acquisition campaign.

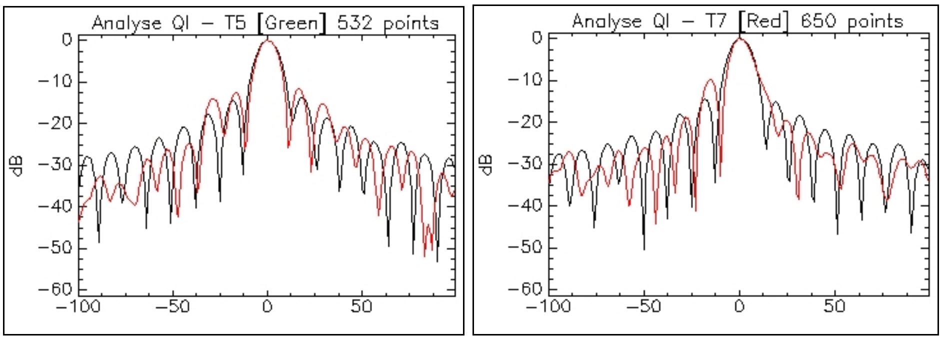

Figure 70 : response of the corner reflectors, T5 (left) and T7 (right) from KaSAR107 image.

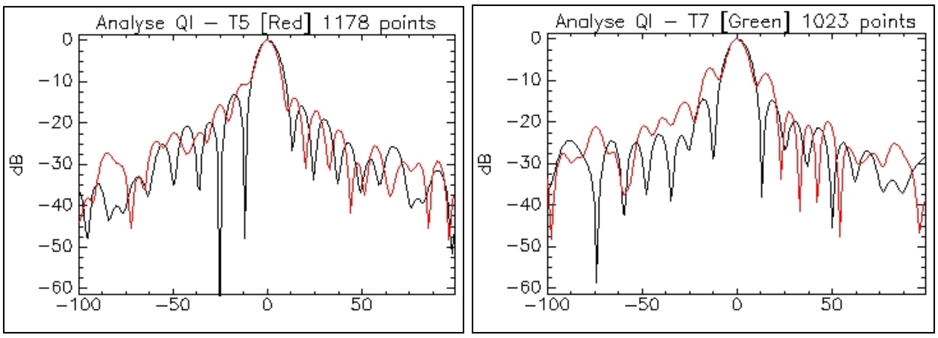

Figure 71 : response of the corner reflectors, T5 (left) and T7 (right) from KaSAR204 image.

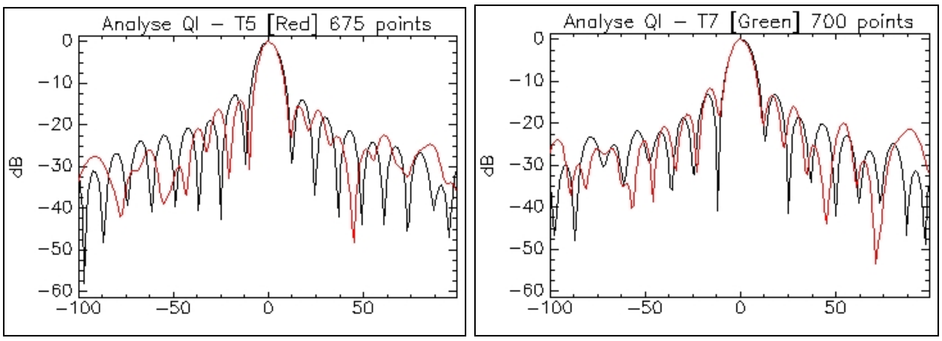

Figure 72 : response of the corner reflectors, T5 (left) and T7 (right) from KaSAR304 image.

3.3.1. Calibration assessment

The analysis of the corner reflectors responses show calibration accuracy within ±0.4 dB except for the trihedral reflector T7 from KaSAR204 image that show a miss-calibration of 1.32 dB.

An upper limit to the Noise Equivalent Sigma0 (NeSigma0) is estimated on the darkest area of each image. The NE sigma0 is equal or better than this value as the darkest area can have a significant Sigma0

image	Darkest area Sigma0 (dB)	Bandwidth	incidence angle (°)
KaSAR103	-23.66	400 MHz	36.59
KaSAR104	-23.71	400 MHz	36.59
KaSAR107	-31.57	400 MHz	32.39
KaSAR204	-25.0	400 MHz	23.47
KaSAR208	-30.75	400 MHz	33.98
KaSAR304	-26.75	400 MHz	21.6
KaSAR308	-36.92	400 MHz	41.43
KaSAR311	-36.95	400 MHz	38.05

Table 26 : Summary of the darkest areas Sigma0 for the DRIVE-BUSARD delivered images.

3.3.2. Structure of delivery disk

The dataset is delivered on a external hard disk labeled ONERA KaSAR data.
Under the top directory, there are several folders containing respectively the ground photos, the in-flight photos, the projected images, the SLC images. Furthermore, one can find the excel file containing the histogram data (KaSAR_histo.xls), the KaSAR file format (KaSAR_file_format.pdf).

The ground photos are organized in two directories, one for the standard pictures and one for the geolocalised pictures. It is then separated by site (St Gilles, Piemanson, Rhone).
The in-flight photos are organized by acquisition.

The projected images are organized by acquisition with the directory name indicating the acquisition identifier, the site and the boresight incidence angle. Each dataset includes a data file and a header (xxx.dat and xxx.ent)

The SLC images are organized similarly to the projected images. One extra file inside the data directory is the mask file, with 1 or 0 depending if the area is in the 6dB round trip illumination pattern. The mask file has the same number of point than the SLC file but is in float and does not have a header.

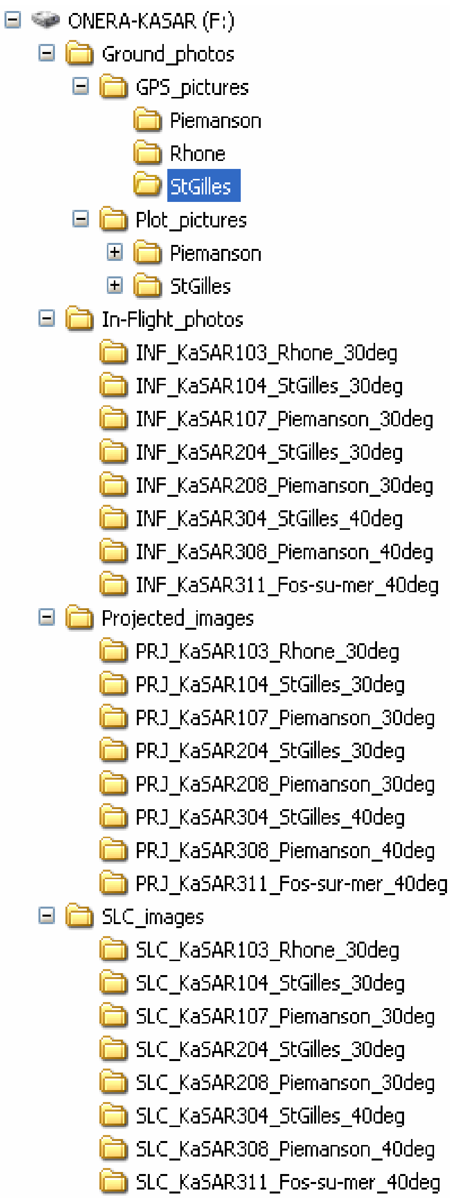

Figure 73 : Structure of the delivery disk. SLC indicates the single look complex files, PRJ stands for projected geometry (WGS84) INF stands for in-flight photos (organised by acquisition) and ground photos are the ground pictures.

3.4. Image analysis

This section is dedicated to the image analysis in terms of Radar Cross Section (RCS) for human made objects or Sigma0 for natural areas. The natural landscapes are composed of sand, different states of sea, short vegetation, trees, orchards, groves and river. The human made areas are industries or towns. Additionally, the histograms of RCS values are plotted for this type of area.

3.4.1. Town and industrial area

The values are presented in radar cross section (RCS) in linear form or in dBm2. One can easily transform a RCS to sigma0 values with the following formula:

$$\sigma_0\,[dBm^2/m^2] = RCS\,[dBm^2] - 10\log_{10}(S_r/\sin\theta)[dBm^2] = RCS - AdB$$

Where Sr is the surface of resolution (0.89 resolution_distance*resolution_azimuth) and q is the incidence angle. AdB is then the normalising surface.

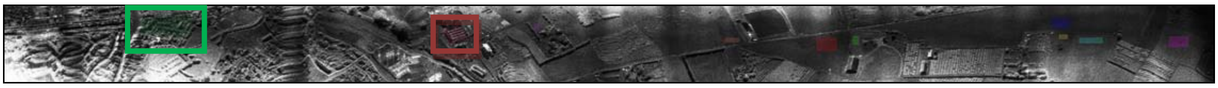

Figure 74 : ROI location on KaSAR104 image.

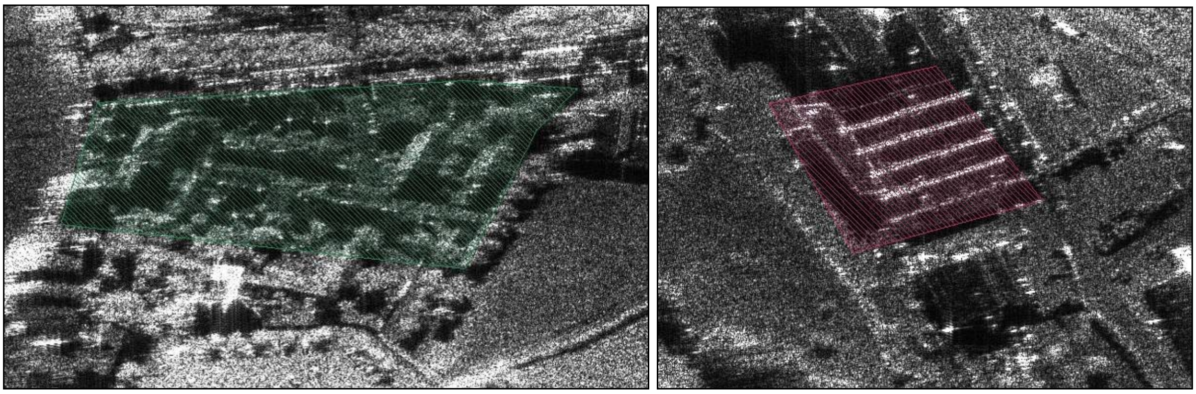

Figure 75 : zoom of KaSAR104 town and industrial area in the green and maroon rectangles respectively (Figure 74) used for the histograms analysis.

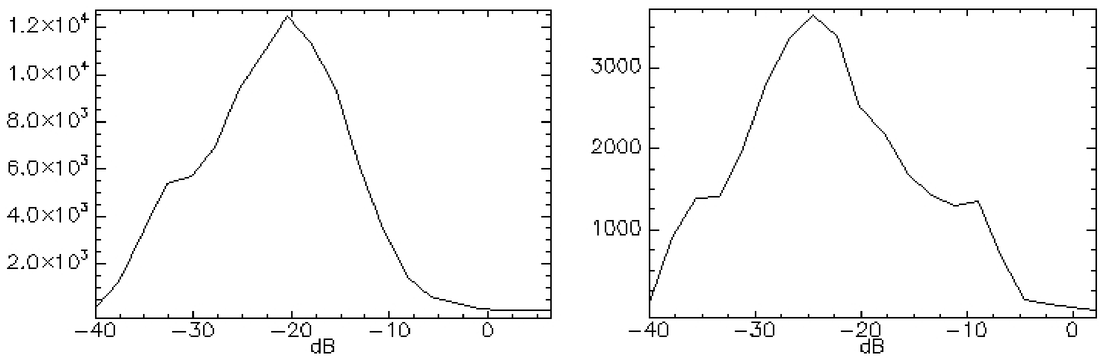

Figure 76 : RCS town (left) and industry (right) histogram from KaSAR104 (Figure 75) image (5x5 multilook => ENL=11.4). AdB= -5.1dB for the town and AdB=-6.4dB for the industrial area.

The histograms are given for multi-look images. For each one the Equivalent Number of Look (ENL) is indicated. The ENL formulation is:

$$ENL = N * \frac{T_{rad} * T_{azi}}{r_{rad} * r_{azi}}$$

Where N is the windowing size (in our case it is 25), T_{rad} and T_{azi} are the pixel spacing along slant range and azimuth axis respectively, r_{rad} and r_{azi} are the slant range and azimuth resolutions.

KaSAR104	Single look		5x5 Multi look, ENL=11,4	
town	RCS mean	RCS std	RCS mean	RCS std
linear	0,064	0,25	0,064	0,15
dB	-11,94		-11,91	

Table 27 : associated mean and standard deviation values from KaSAR104 (single and 5x5 multilook).

KaSAR104	Single look		5x5 Multi look, ENL=11,4	
industry	RCS mean	RCS std	RCS mean	RCS std
linear	0,082	0,32	0,082	0,17
dB	-10,86		-10,86	

Table 28 : associated mean and standard deviation values from KaSAR104 (single and 5x5 multilook).

Figure 77 : ROI location on KaSAR204 image.

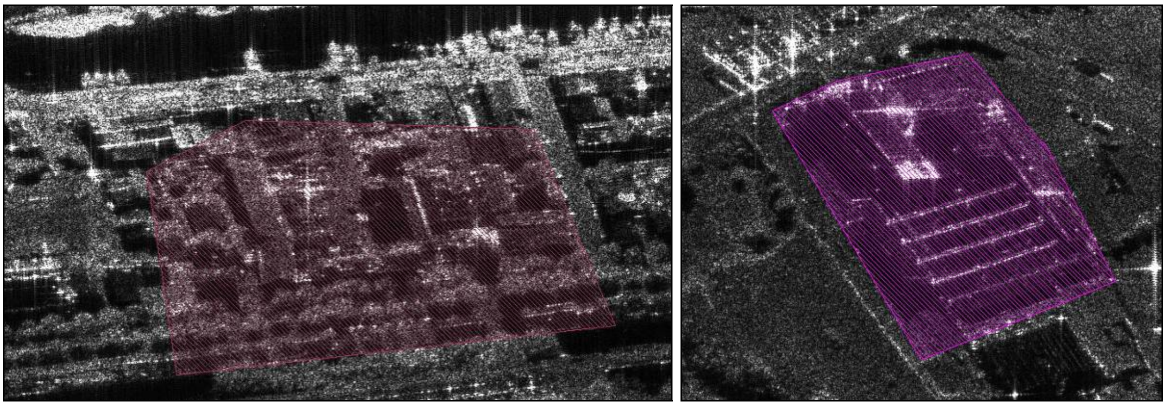

Figure 78 : zoom of KaSAR204 town and industrial area in the green and maroon rectangles respectively (Figure 77) used for the histograms analysis.

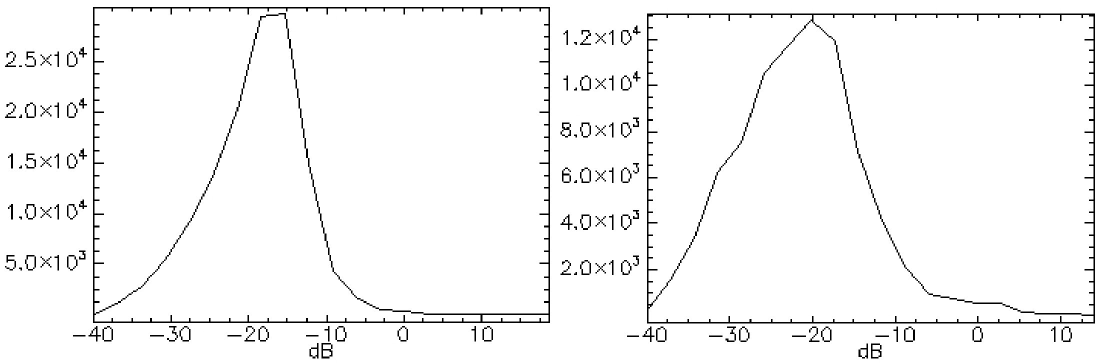

Figure 79 : RCS town (left) and industry (right) histogram from KaSAR204 (Figure 78) image (5x5 multilook => ENL=11.4). AdB= -5.4dB for the town and AdB=-6.2dB for the industrial area.

KaSAR204	Single look		5x5 Multi look, ENL=11,4	
town	RCS mean	RCS std	RCS mean	RCS std
linear	0,19	4,72	0,19	1,94
dB	-7,23		-7,22	

Table 29 : associated mean and standard deviation values from KaSAR204 (single and 5x5 multilook).

KaSAR204	Single look		5x5 Multi look, ENL=11,4	
industry	RCS mean	RCS std	RCS mean	RCS std
linear	0,2	2,69	0,2	1,35
dB	-6,92		-6,92	

Table 30 : associated mean and standard deviation values from KaSAR204 (single and 5x5 multilook)

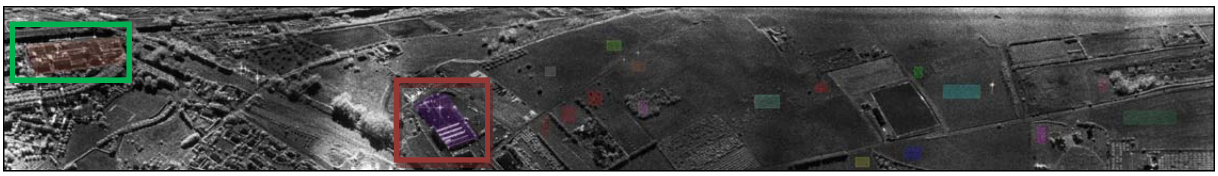

Figure 80 : ROI location on KaSAR304 image.

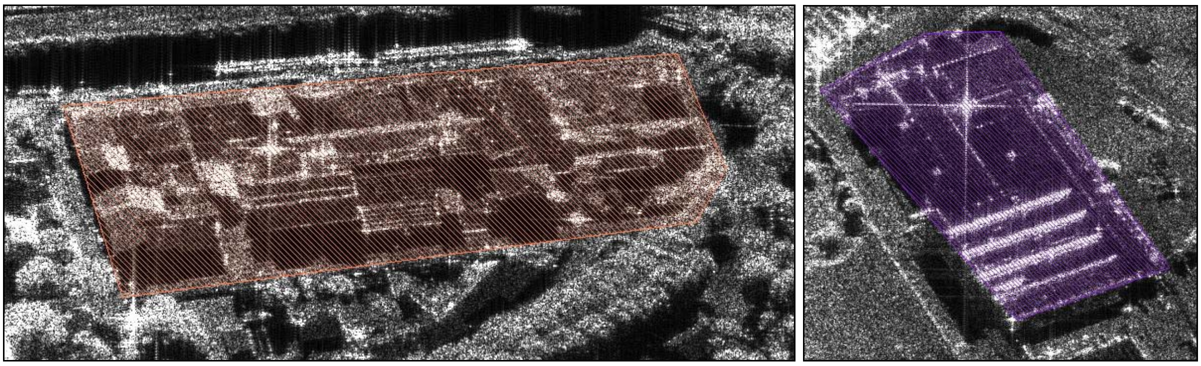

Figure 81 : zoom of KaSAR304 town and industrial area in the green and maroon rectangles respectively (Figure 80) used for the histograms analysis.

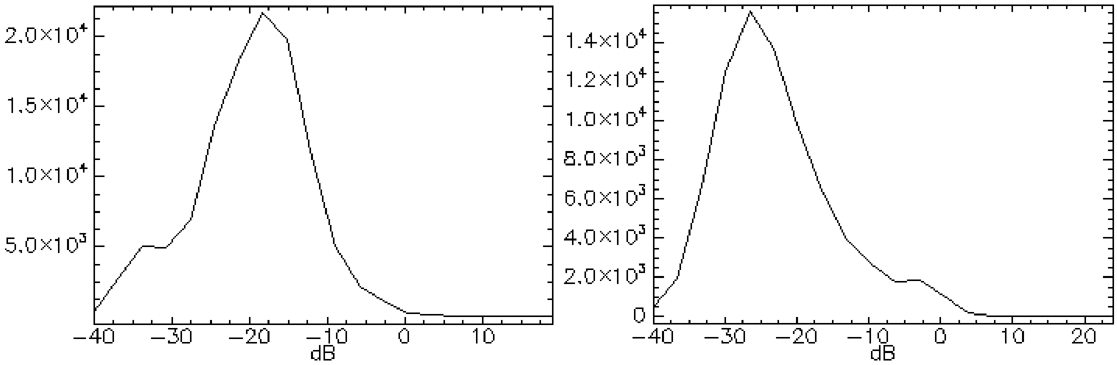

Figure 82 : RCS town (left) and industry (right) histogram from KaSAR304 (Figure 81) image (5x5 multilook => ENL=11.4). AdB= -6.5 dB for the town and AdB=-7.4dB for the industrial area.

KaSAR304	Single look		5x5 Multi look, ENL=11,4	
town	RCS mean	RCS std	RCS mean	RCS std
linear	0,16	4,88	0,16	2,16
dB	-8,02		-8,02	

Table 31 : associated mean and standard deviation values from KaSAR304 (single and 5x5 multilook)

KaSAR304	Single look		5x5 Multi look, ENL=11,4	
industry	RCS mean	RCS std	RCS mean	RCS std
linear	0,43	24,61	0,43	8,64
dB	-3,64		-3,64	

Table 32 : associated mean and standard deviation values from KaSAR304 (single and 5x5 multilook).

As noted on the archive data analysis, the spread of values is very high over anthropogenic areas with very dark pixels (associated with shadows) and very bright pixels (associated with multi-bounce scattering).

3.4.2. Vegetation

The ROI's over the St Gilles area are identified in Figure 83. They include short vegetation, forest, orchards… which will be analyzed in the next paragraphs. The Sigma0 values associated with each of them is reported when the illumination conditions are adequate (field inside the mask)

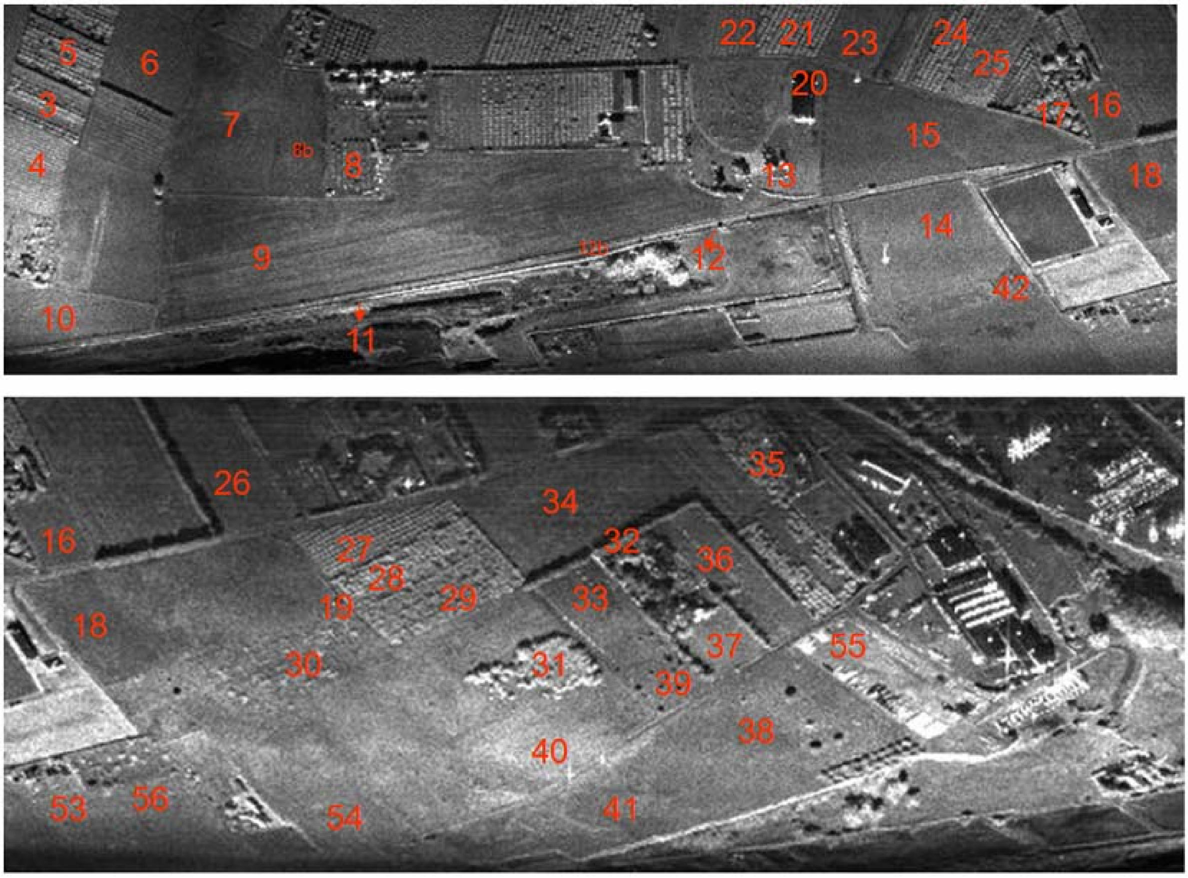

Figure 83 : ROI definition over St Gilles.

ROI ID	Description
1	Cut trees
2	Alfalfa field
3	Orchards 3m apricot
4	Young apricot trees, 1.5m
5	Apricot trees
6	Vineyard
7	Grazing field
8	Olive tree + shelter + enclosure
9	Cut wheat field
10	Vineyard
11	Tree along road + heavy grating. Zone is around 20m below road, with water at the bottom.
12	Corner of the enclosed area with electric shelter

13	Houses
14	Grazing area
15	Grazing area + fallow
16	High fallow (0.8m)
17	Cherry trees
18	High fallow (0.8m)
19	Small shelter
20	Big industrial shed
21	Old orchard (apricot) 2.5m
22	young orchard (apricot) 1.2m
23	Fallow
24	Old orchard (apricot) 2.5m + olive trees between 23 and 24 + 2 rows of young orchard
25	Old orchard
26	Grazing field
27	Young orchard
28	Old orchard + small shed
29	Old orchard
30	Dead orchard
31	Tree grove 4.7m
32	Cypress hedge
33	Grazing
34	Grazing
35	Orchard
36	Bare soil
37	Low grazing
38	Fallow 0.5m
39	Grass with young pine trees
40	Fallow
41	Fallow
42	Young trees
44	Municipal park with grass + olive trees
45	Grass area + pine trees
46	Grass in a low basin
47	High grass in a lower area
48	Grass
49	Lawn area + children park
50	Parking on gravel
51	Vegetable growing field
52	Parking
53	Bare soil + 53Fallow (0.3 to 0.4m)
54	Bare soil
55	Industrial storage area
56	Fallow – traces of furrows – Green clump of vegetation

Table 33 : type of area according to the ROI definition over St Gilles.

Following ESA suggestions, we have computed an average behaviour over the agricultural area of St Gilles. The averaging is performed over the pixels for which the mask value is 1, in order to reject areas of non reliable calibration. **Figure 84** plots the mean sigma0 profiles for the natural landscape over St Gilles computed over a large area and taking into account the image mask.

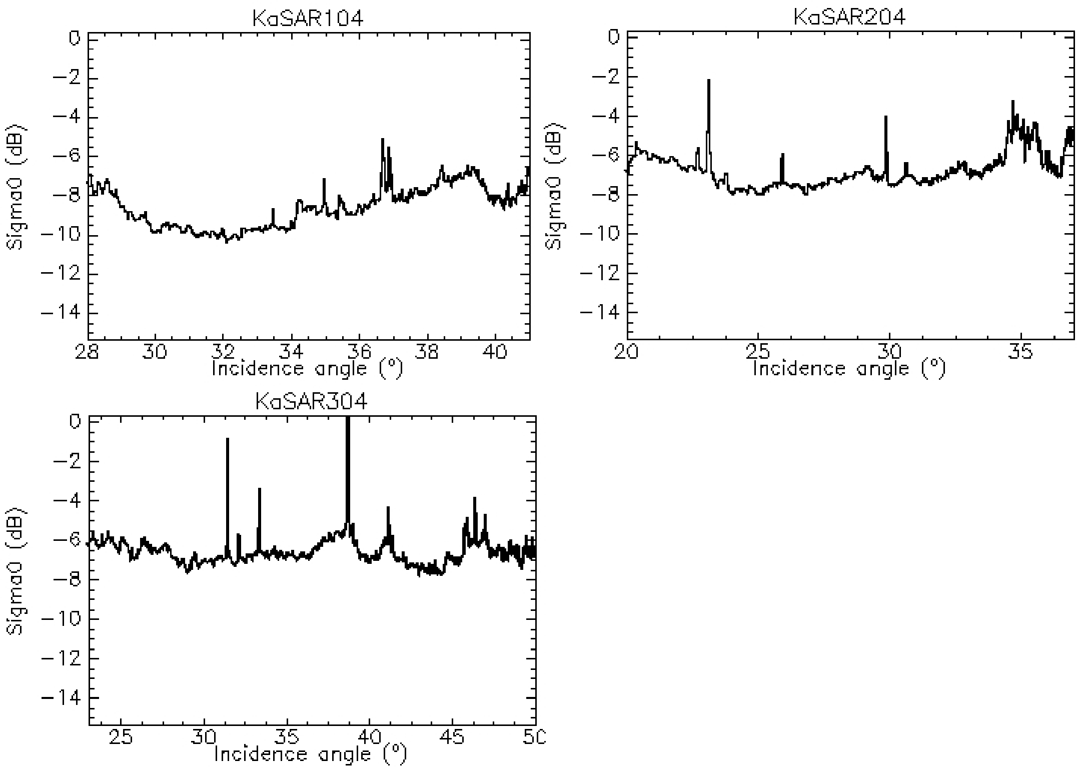

Figure 84 : Sigma0 mean value over the natural landscape of St Gilles area, depending on the incidence angle.

For vegetation and agricultural areas, for incidence ranging from 20 to 50°, we note an almost flat curve with incidence angle, with a value around -7dB. This is typical of rough surfaces (or very rough).

3.4.2.1. Short vegetation

In the previous plots, we did not select any particular type of field, but consider the variety of crops found in the St Gilles area. We now refine the analysis by considering only the short vegetation area which can be grazing fields, abandoned fields, grassy areas…

ROI N°	type of area	image	Polarization	incidence angle	Sigma0 (dB)	Sigma0 (lin)	Sigma0 Std (lin)
7	short vegetation	KaSAR104	Vv	36,83	-7,8	0,17	0,17
8b	short vegetation	KaSAR104	Vv	35,84	-9,18	0,12	0,12
9	short vegetation	KaSAR104	Vv	31,79	-11,71	0,07	0,07
15	short vegetation	KaSAR104	Vv	37,78	-9,14	0,12	0,13
18	short vegetation	KaSAR104	Vv	36,74	-9,78	0,11	0,11
37	short vegetation	KaSAR104	Vv	33,2	-6,51	0,22	0,23
9	short vegetation	KaSAR204	Vv	32,01	-9,66	0,11	0,12
14	short vegetation	KaSAR204	Vv	29,89	-8,03	0,16	0,17
18	short vegetation	KaSAR204	Vv	29,4	-7,51	0,18	0,19
38	short vegetation	KaSAR204	Vv	27,6	-8,28	0,15	0,15

40	short vegetation	KaSAR204	Vv	25,64	-6,93	0,20	0,21
54	short vegetation	KaSAR204	Vv	21,02	-8,72	0,13	0,14
9	short vegetation	KaSAR304	Vv	42,08	-7,41	0,18	0,20
14	short vegetation	KaSAR304	Vv	37,55	-7,15	0,19	0,20
15	short vegetation	KaSAR304	Vv	46,96	-7,76	0,17	0,18
16	short vegetation	KaSAR304	Vv	48	-8,49	0,14	0,15
18	short vegetation	KaSAR304	Vv	36,83	-8,22	0,15	0,16
36	short vegetation	KaSAR304	Vv	43,54	-5,3	0,30	0,33
37	short vegetation	KaSAR304	Vv	41,66	-6,13	0,24	0,25
38	short vegetation	KaSAR304	Vv	33,24	-9,42	0,11	0,13
40	short vegetation	KaSAR304	Vv	31,98	-6,62	0,22	0,22
41	short vegetation	KaSAR304	Vv	25,63	-9,88	0,10	0,11

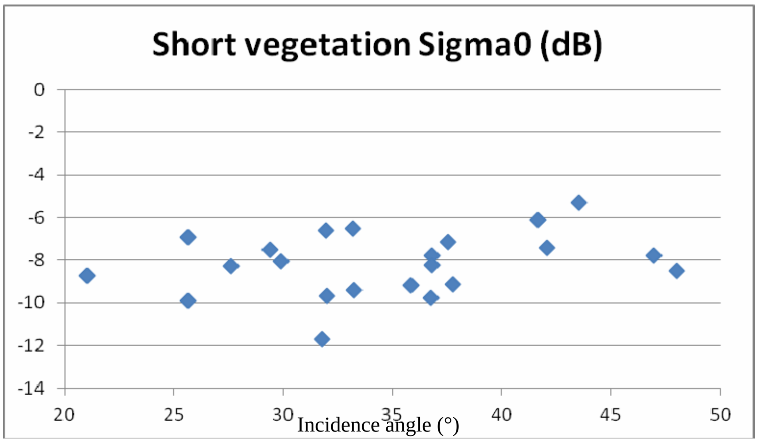

Figure 85 : Short vegetation Sigma0 plot in dB according to the incidence angle.

The short vegetation areas are characterized by a constant behavior with incidence angle, with an averaged value around -8dB. Furthermore, the statistics indicates that there are homogeneous areas, with the standard deviation following closely the mean value as expected from a homogeneous area in a single look complex image.

3.4.2.2. Trees/Groves/Orchard

ROI N°	type of area	image	Polarization	incidence angle	Sigma0 (dB)	Sigma0 (lin)	Sigma0 Std (lin)
4	trees/groves/orchard	KaSAR104	Vv	37,18	-8,95	0,13	0,14
42	trees/groves/orchard	KaSAR204	Vv	26,75	-11,01	0,08	0,09
39	trees/groves/orchard	KaSAR204	Vv	31,06	-7,92	0,16	0,20
42	trees/groves/orchard	KaSAR304	Vv	33,38	-9,45	0,11	0,13
30	trees/groves/orchard	KaSAR304	Vv	39,44	-9,42	0,11	0,15
31	trees/groves/orchard	KaSAR304	Vv	40,38	-5,78	0,26	0,32
39	trees/groves/orchard	KaSAR304	Vv	38,85	-8,35	0,15	0,17

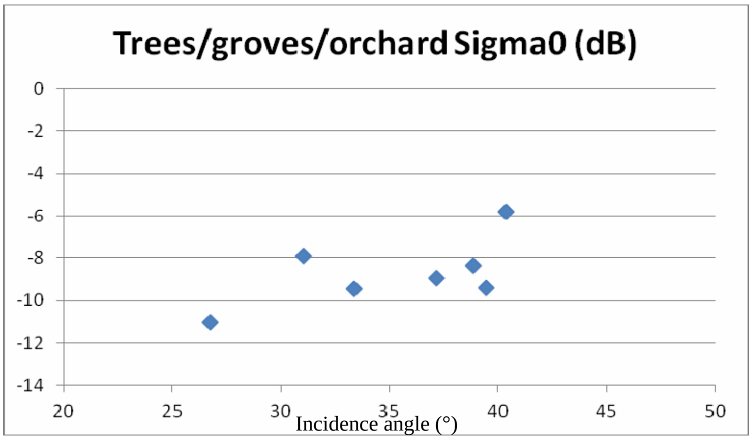

Figure 86 : Highest vegetation Sigma0 plot in dB according to the incidence angle.

Only a few plots of trees are present in the data. The values are ranging from -11dB to -6dB. No conclusion can be drawn for the trend with incidence angle because of the high variability in the type of trees (pine tree, fruit trees) and the limited number of points.

3.4.2.3. Sea and Sand

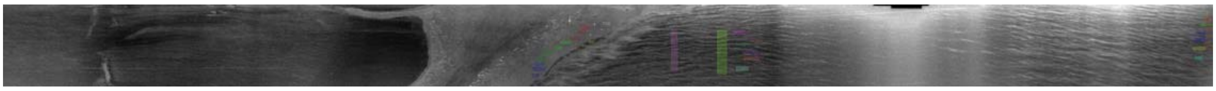

Figure 87 : ROI location on KaSAR107 image.

Figure 88 : ROI location on KaSAR208 image.

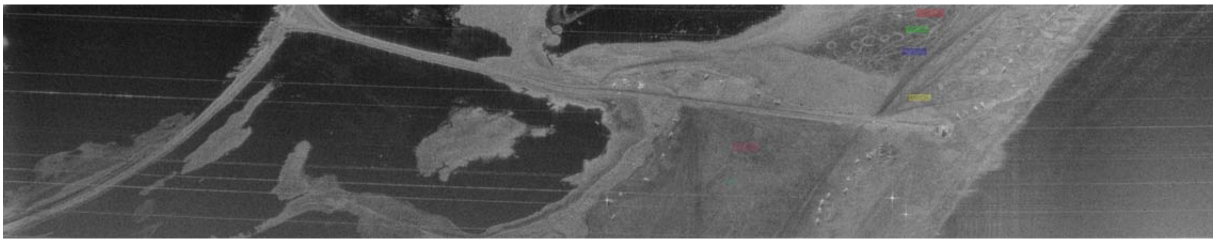

Figure 89 : ROI location on KaSAR308 image.

As explained above, the first data acquisition took place on a windy day where the sea surface was rough with wind gusts up to 45km/h. In **Figure 77**, the wave pattern can clearly be seen on the right of the image. The water surface on the left of the image is a marsh area, with smoother water.

We followed the same approach as before and we averaged large sea areas in order to provide information on the overall trend of backscatter with incidence angle. As before, we only averaged pixel inside the radiometry mask.

For the sea backscatter, we observe a different behaviour for the rough sea (first flight, KaSAR107, wind at 25km/h with gust at 45km/h)) and a smooth sea (second flight, KaSAR208). For rough sea, the sigma0 is steadily decreasing with incidence angle whereas over the smooth sea, the profile is increasing with incidence angle, a behaviour which is typical of a noise dominated signal and can be encountered when the signal is very low (very smooth surface) and equivalent to the noise level.

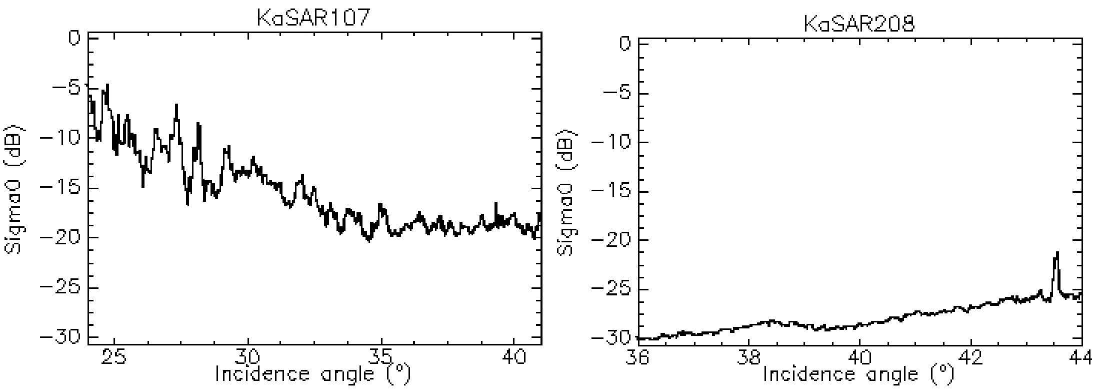

Figure 90 : Sigma0 mean value over the sea of Piemanson area, depending on the incidence angle.

3.4.2.4. Rough sea

The rough sea regions of interest are identified in **Figure 87**. The exact location of these ROIs is not essential but what is important is the observed decreasing backscattering value with incidence angle.

ROI N°	type of area	image	Polarization	incidence angle	Sigma0 (dB)	Sigma0 (lin)	Sigma0 Std (lin)
1	rough sea	KaSAR107	Vv	25,84	-10,34	0,09	0,15
2	rough sea	KaSAR107	Vv	28,17	-13,69	0,04	0,07
3	rough sea	KaSAR107	Vv	31,86	-15,43	0,03	0,04
4	rough sea	KaSAR107	Vv	35,05	-16,4	0,02	0,03
5	rough sea	KaSAR107	Vv	37,25	-14,58	0,03	0,04
6	rough sea	KaSAR107	Vv	30,55	-14,25	0,04	0,06
7	rough sea	KaSAR107	Vv	32,76	-17,99	0,02	0,03
8	rough sea	KaSAR107	Vv	33,99	-15,67	0,03	0,05
9	rough sea	KaSAR107	Vv	36,03	-21,99	0,01	0,01
10	rough sea	KaSAR107	Vv	37,4	-21,06	0,01	0,01
11	rough sea	KaSAR107	Vv	39,52	-17,92	0,02	0,02

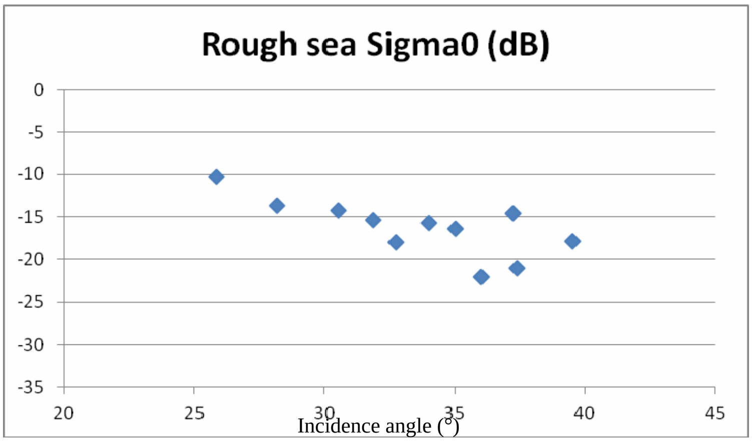

Figure 91 : Rough sea Sigma0 plot in dB according to the incidence angle.

Figure 92 : Zoom on rough sea from KaSAR107 image (left) and associated optical image acquired simultaneously by onboard camera.

In **Figure 92**, the wave pattern can clearly be seen in the radar image. This wave modulation can clearly be seen in the following plot which corresponds to the backscatter profile as a function of incidence angle for the three elongated ROIS in **Figure 87**.

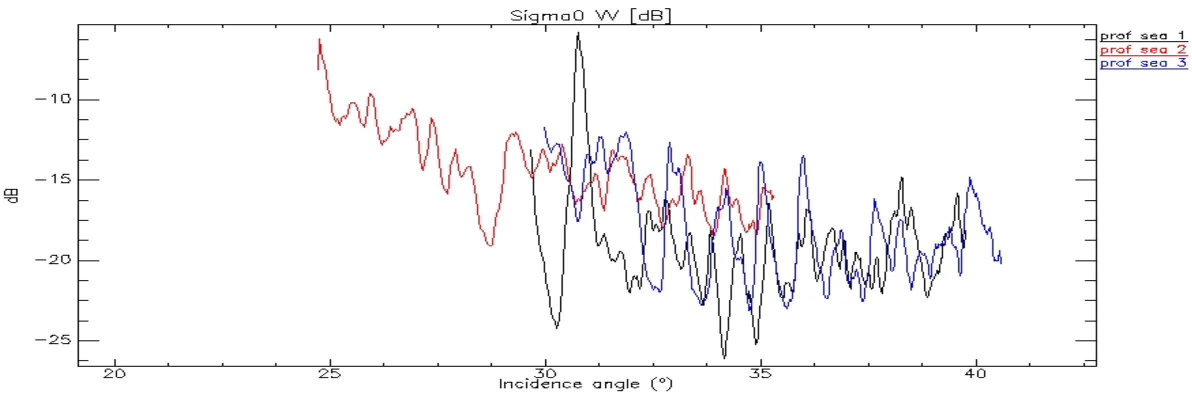

Figure 93 : Profiles on rough sea from KaSAR107 image.

3.4.2.5. Smooth sea

As noted earlier, on the second and third flight the water was very smooth and the corresponding backscatter very low. As a result, we observe that the backscatter values are increasing with incidence angle. We believe this is an artefact linked to an increasing Noise-Equivalent Sigma0 which as expected increases with increasing range and to an antenna pattern effect when moving off the boresight antenna pattern.

ROI N°	type of area	image	Polarization	incidence angle	Sigma0 (dB)	Sigma0 (lin)	Sigma0 Std (lin)
1	smooth sea	KaSAR208	Vv	31,78	-29,21	0,0012	0,0010
2	smooth sea	KaSAR208	Vv	33,24	-28,27	0,0015	0,0013
3	smooth sea	KaSAR208	Vv	34,54	-28,96	0,0013	0,0010
4	smooth sea	KaSAR208	Vv	36,04	-28,32	0,0015	0,0013
5	smooth sea	KaSAR208	Vv	37,43	-27,1	0,0019	0,0015
6	smooth sea	KaSAR208	Vv	38,61	-29,74	0,0011	0,0009
7	smooth sea	KaSAR208	Vv	40,87	-26,7	0,0021	0,0019
8	smooth sea	KaSAR208	Vv	42,35	-24,16	0,0038	0,0036
9	smooth sea	KaSAR208	Vv	40,54	-27,92	0,0016	0,0014
10	smooth sea	KaSAR208	Vv	41,8	-27,11	0,0019	0,0016
11	smooth sea	KaSAR208	Vv	43,03	-25,67	0,0027	0,0021

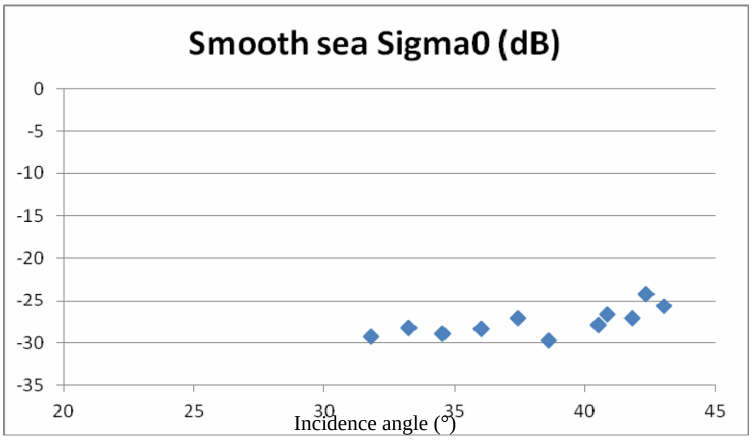

Figure 94 : Smooth sea Sigma0 plot in dB according to the incidence angle.

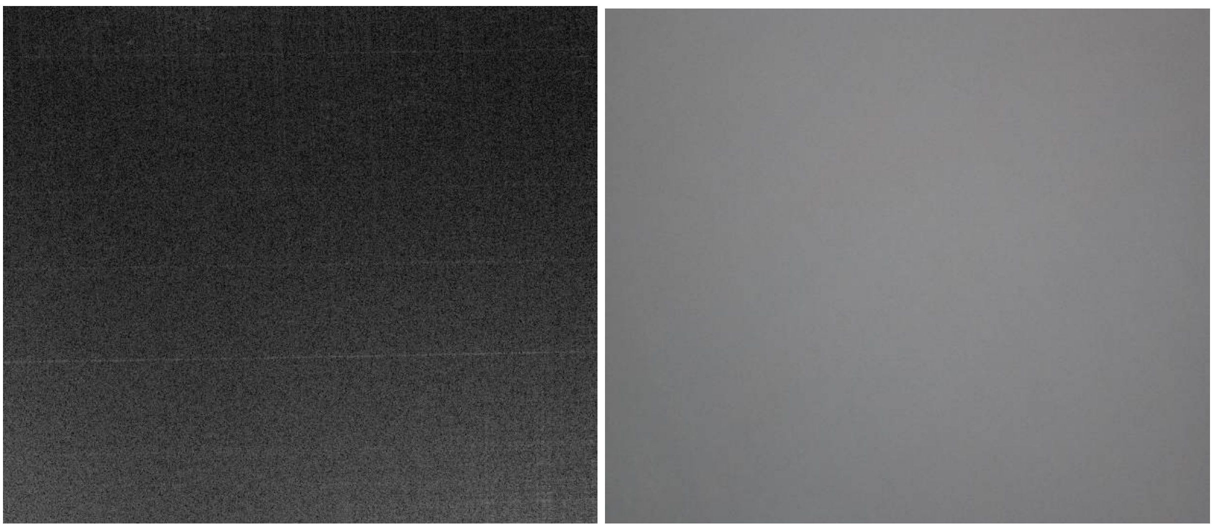

Figure 95 : Zoom on smooth sea from KaSAR208 image (left) and associated optical image acquired simultaneously by onboard camera.

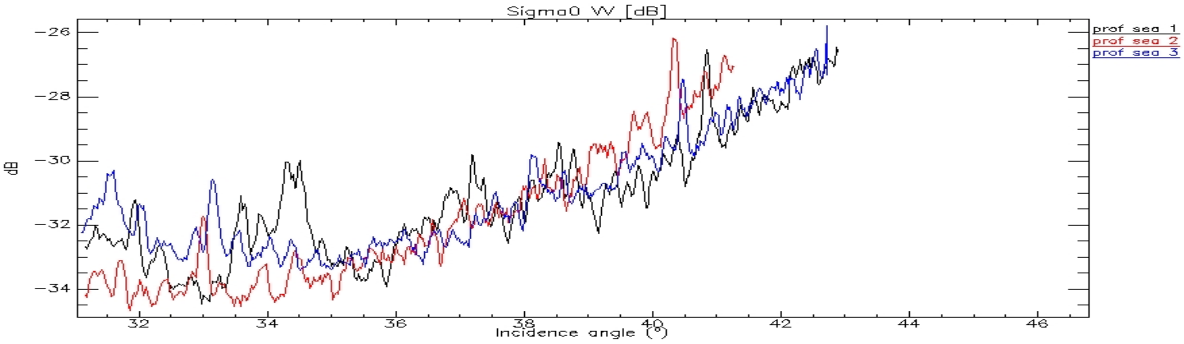

Figure 96 : Profiles on smooth sea from KaSAR208 image.

3.4.2.6. Sand

The wet sand areas are areas which are regularly covered with water. As a result, there are smoother than the dry sand areas.

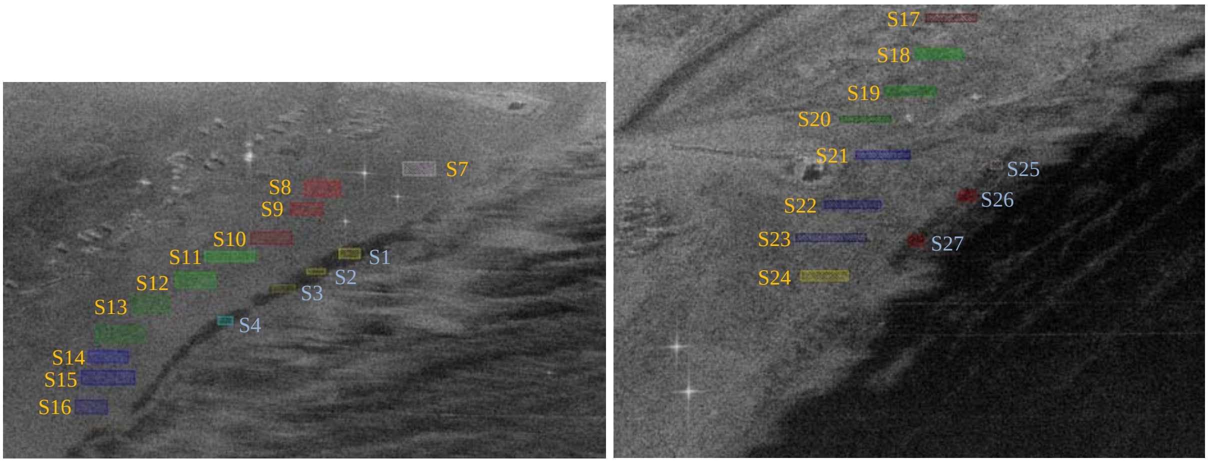

Figure 97 : Sand ROIs location for KaSAR107 (left), for KaSAR208 (right).

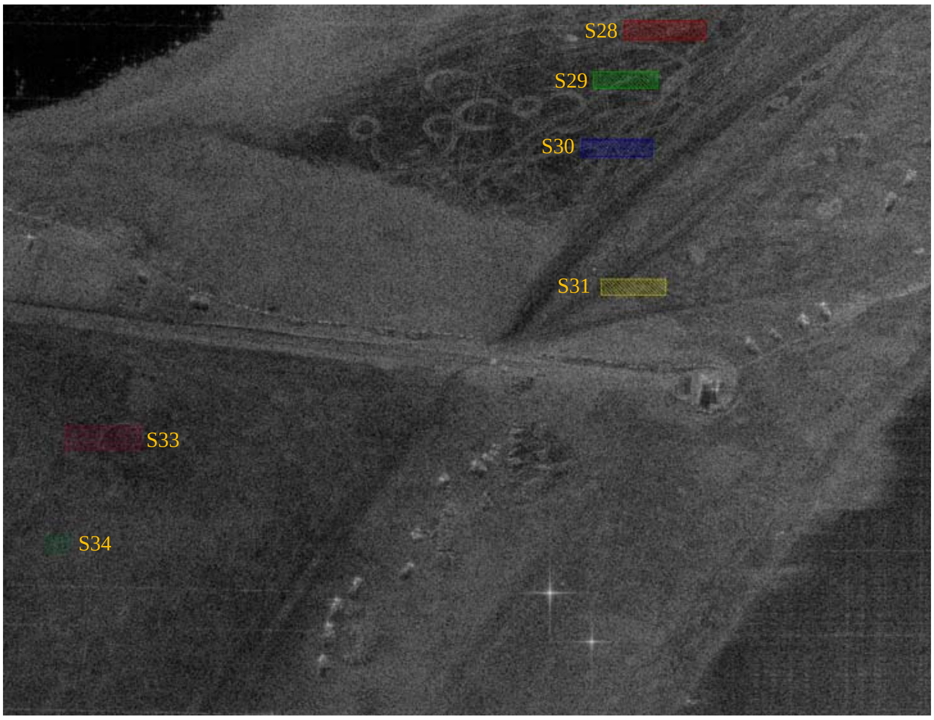

Figure 98 : Sand ROIs for KaSAR308.

ROI N°	type of area	image	Polarization	incidence angle	Sigma0 (dB)	Sigma0 (lin)	Sigma0 Std (lin)
S1	wet sand	KaSAR107	Vv	33,34	-22,15	0,0061	0,0084
S2	wet sand	KaSAR107	Vv	34,38	-21,45	0,0072	0,0086
S3	wet sand	KaSAR107	Vv	35,29	-19,62	0,0109	0,0154
S4	wet sand	KaSAR107	Vv	36,95	-20,93	0,0081	0,0084
S25	wet sand	KaSAR208	Vv	38,41	-19,06	0,0124	0,0186
S26	wet sand	KaSAR208	Vv	40,53	-18,73	0,0134	0,0183
S27	wet sand	KaSAR208	Vv	41,24	-18,85	0,0130	0,0162

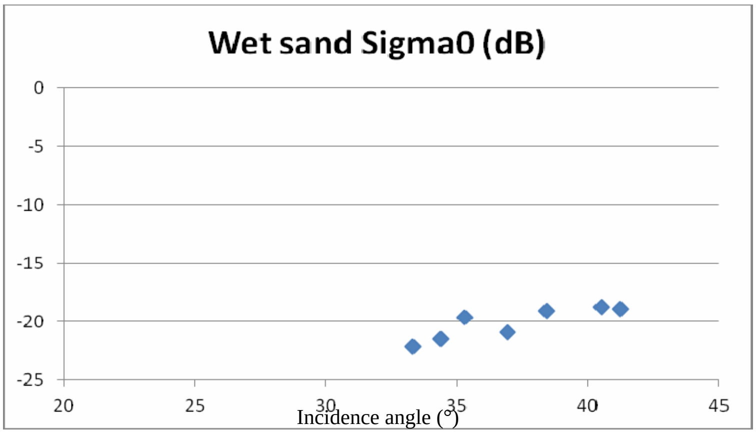

Figure 99 : Wet sand Sigma0 plot in dB according to the incidence angle.

ROI N°	type of area	image	Polarization	incidence angle	Sigma0 (dB)	Sigma0 (lin)	Sigma0 Std (lin)
S7	dry sand	KaSAR107	Vv	27,58	-11,63	0,0687	0,0774
S8	dry sand	KaSAR107	Vv	29,1	-12,86	0,0518	0,0527
S9	dry sand	KaSAR107	Vv	30,53	-13,26	0,0472	0,0497
S10	dry sand	KaSAR107	Vv	32,4	-12,48	0,0565	0,0562
S11	dry sand	KaSAR107	Vv	33,52	-12,45	0,0569	0,0551
S12	dry sand	KaSAR107	Vv	34,84	-12,07	0,0621	0,0647
S13	dry sand	KaSAR107	Vv	36,89	-12,63	0,0546	0,0579
S14	dry sand	KaSAR107	Vv	38,66	-12,74	0,0532	0,0560
S15	dry sand	KaSAR107	Vv	39,58	-13,42	0,0455	0,0457
S16	dry sand	KaSAR107	Vv	40,82	-12,42	0,0573	0,0593
S17	dry sand	KaSAR208	Vv	31,62	-5,16	0,3048	0,4532
S18	dry sand	KaSAR208	Vv	32,83	-6,16	0,2421	0,2681
S19	dry sand	KaSAR208	Vv	34,35	-8,11	0,1545	0,1770
S20	dry sand	KaSAR208	Vv	35,14	-6,28	0,2355	0,2999
S21	dry sand	KaSAR208	Vv	37,01	-8,06	0,1563	0,1915
S22	dry sand	KaSAR208	Vv	38,66	-8,84	0,1306	0,1469
S23	dry sand	KaSAR208	Vv	39,83	-9,63	0,1089	0,1238
S24	dry sand	KaSAR208	Vv	41,35	-10,08	0,0982	0,1113
S28	dry sand	KaSAR308	Vv	37,42	-13,95	0,0403	0,0551
S29	dry sand	KaSAR308	Vv	39,61	-15,91	0,0256	0,0384
S30	dry sand	KaSAR308	Vv	42,25	-15,49	0,0282	0,0388
S31	dry sand	KaSAR308	Vv	46,76	-11,38	0,0728	0,1029
S33	dry sand	KaSAR308	Vv	50,65	-18,38	0,0145	0,0189
S34	dry sand	KaSAR308	Vv	52,95	-14,573	0,0349	0,0376

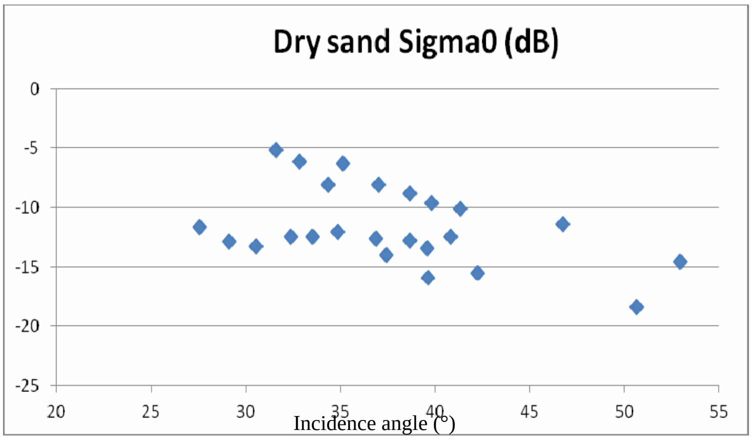

Figure 100 : Dry sand Sigma0 plot in dB according to the incidence angle.

In the dry sand areas, we can find a large variety of roughness. As a result the spread of backscatter is large and was observed to range 8dB for some cases. The overall trend is decreasing with incidence angle as expected.

3.4.3. River

Figure 101 : ROI location on KaSAR103 image.

ROI N°	type of area	image	Polarization	incidence angle	Sigma0 (dB)	Sigma0 (lin)	Sigma0 Std (lin)
S35	river	KaSAR103	Vv	23,91	-11,9	0,0646	0,0246
S36	river	KaSAR103	Vv	24,87	-16,8	0,0209	0,0145
S37	river	KaSAR103	Vv	26,87	-19,69	0,0107	0,0115
S38	river	KaSAR103	Vv	29,19	-20,34	0,0092	0,0076
S39	river	KaSAR103	Vv	31,24	-22,31	0,0059	0,0054
S40	river	KaSAR103	Vv	33,44	-23,47	0,0045	0,0054
S41	river	KaSAR103	Vv	34,66	-24,53	0,0035	0,0046

Figure 102 : Zoom on river from KaSAR103 image (left) and associated optical image acquired simultaneously by onboard camera.

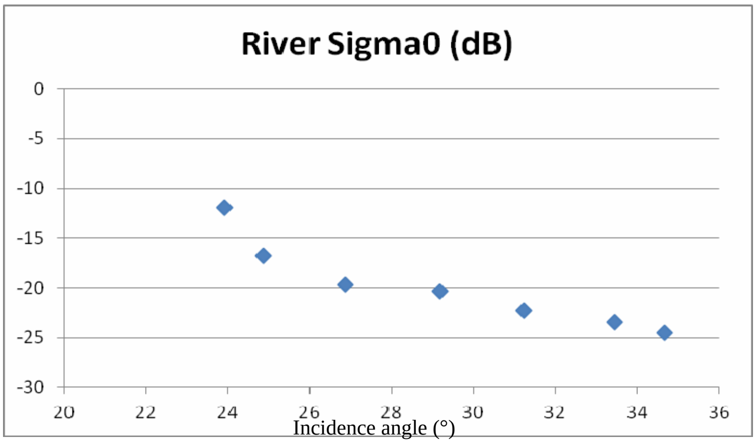

Figure 103 : Rhone river Sigma0 plot in dB according to the incidence angle.

During the first flight, the wind was blowing strongly on the Camargue area. The Rhone river surface is affected by this wind as can be seen in the wave pattern. The river surface is smoother on the side of the river as the banks are acting as a protecting bareer for the wind. The values are very similar to the one observed in the sea.

3.4.4. Comparison with other datasets

To complete the Sigma0 measurements, we compare the data acquired by RAMSES, by DRIVE-BUSARD and the values given by Ulaby in REF-6 when they exist. The plots are presented for different landscapes.
The first comparison (Figure 104) concerns the short vegetation over St Gilles area. The red points correspond to the DRIVE-BUSARD Vv data, The Blue points is the RAMSES Hh and Vv data and the green ones the Ulaby Vv values (5% and 95% occurrence level). This plot shows that all the measurements from RAMSES and DRIVE-BUSARD are within the Ulaby 5%-95% limits.

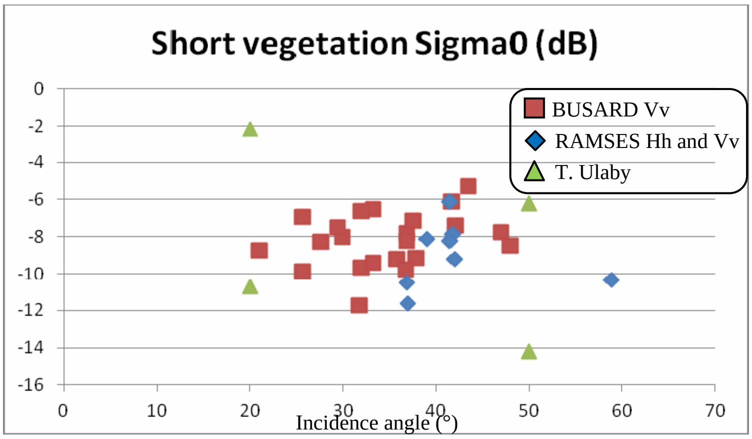

Figure 104 : comparison of short vegetation Sigma0. Plot is in dB according to the incidence angle.

Figure 105 plots the Sigma0 measurements for DRIVE-BUSARD and RAMSES acquisitions and the Ulaby min and max values for taller vegetation. For this kind of vegetation it appears that the Ulaby values for trees and the measurements on SLC do not match very well. The measured values from the DRIVE-BUSARD data for the trees and for an incidence angle of 40° is -5.78dB (ROI31, Figure 106) but Ulaby sigma0 mean value for Vv polarization for the same incidence is -12.7dB. DRIVE-BUSARD data sigma0 measurements for trees are much higher than those from Ulaby handbook.

It is interesting to note that the Sigma0 values for trees in Ulaby's handbook are lower than the values associated with short vegetation. In the DRIVE-BUSARD dataset, we observe that the sigma0 values for short vegetation and forest can be very similar. This is illustrated on the image from St Gilles (Figure 106) where the intensity of the image does not show a strong contrast between the trees (ROI 31) and the surrounding grass (ROI 40 or 41). In fact, the tree plot is visible because it generates a shadow at its border and has a distinctive texture.

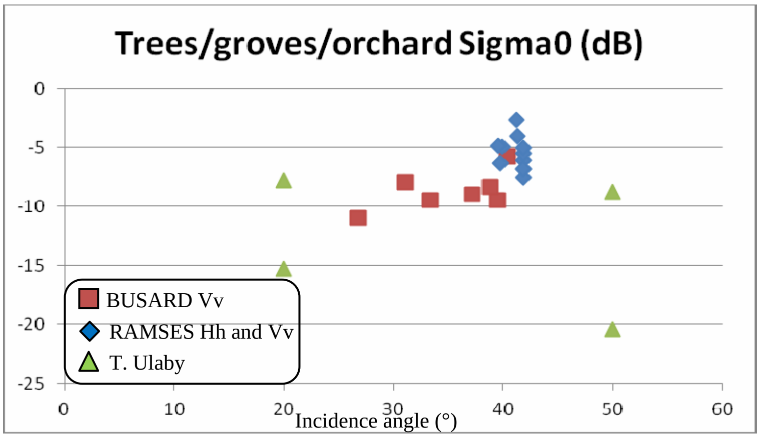

Figure 105 : comparison of highest vegetation Sigma0. Plot is in dB according to the incidence angle.

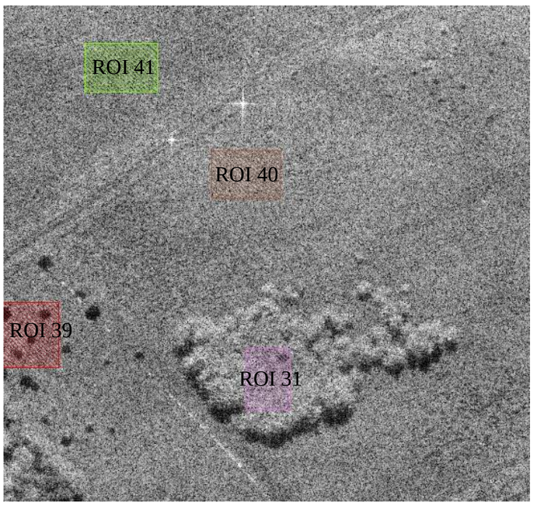

Figure 106 : KaSAR304 magnitude image extraction.

Figure 107 presents the cross-platform sigma0 comparison for different states of the sea. DRIVE-BUSARD Vv data for rough sea is plotted in red, for smooth sea in green and RAMSES Vv data for rough sea in blue. The plot illustrates the wide variation in sigma0 depending on the state of the sea.

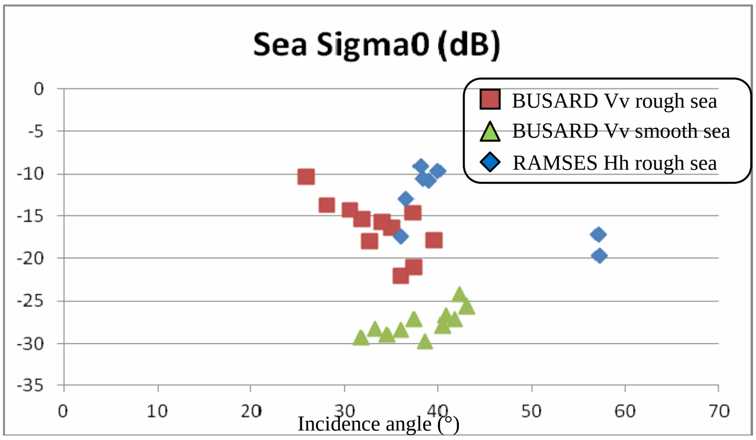

Figure 107 : comparison of sea Sigma0. Plot is in dB according to the incidence angle.

Figure 108 presents the cross-platform Sigma0 comparison for sand measurements from RAMSES (blue points) and DRIVE-BUSARD (red and green points) data. A wide variation of Sigma0 is observed. We believe it is mostly linked to the surface roughness of the sand (the wet sand is regularly covered with water) and potentially with soil moisture.

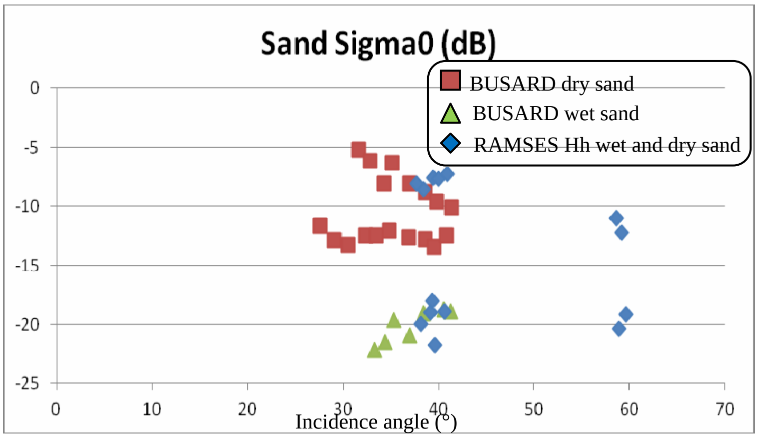

Figure 108 : comparison of sand Sigma0. Plot is in dB with respect to the incidence angle.

3.4.5. Vehicle extraction

Vehicles detection is an important topic for security applications. This section analyses the contrast between vehicles and their surrounding in terms of Sigma0. The contrast is defined as the sigma0 difference between vehicle and surrounding.
Figure 109 and Figure 110 are extractions from the delivered dataset. Ever though the vehicle can be seen on the image, this is mostly due to the shape and the shadow. A very poor sigma0 contrast between the vehicle and the surrounding clutter is observed. The table confirms the poor contrast and gives the associated Sigma0.

Figure 109 : extraction from KaSAR304 image of vehicles (left) and the corresponding picture acquired simultaneously by onboard camera (right).

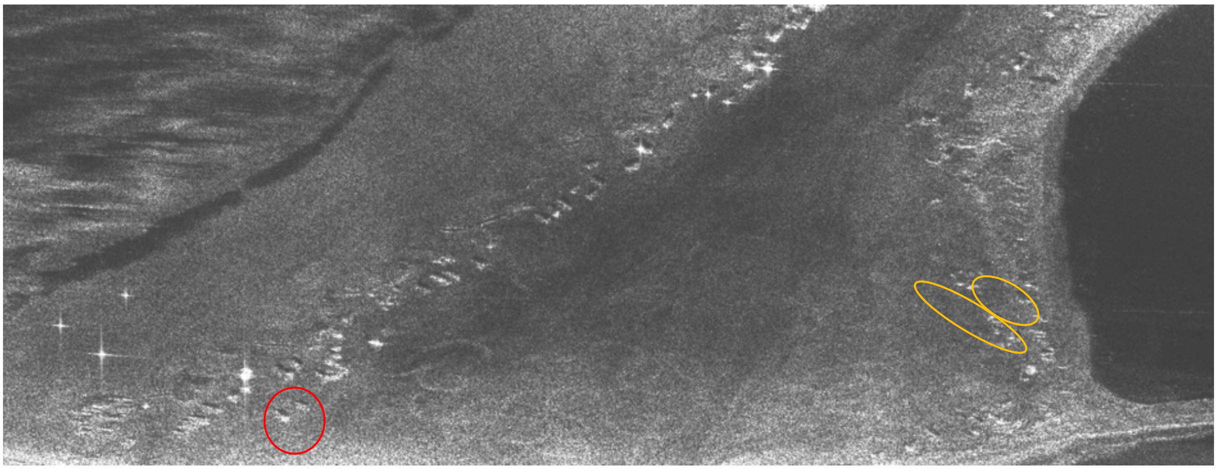

Figure 110 : extraction from KaSAR107 image of vehicles and the corresponding picture acquired simultaneously by onboard camera is presented below (Figure 111).

Figure 111 : Picture acquired simultaneously with the SAR image (presented Figure 110) by onboard camera. The red circles are positioned to identify the same two cars in the two images.

Figure 112 : extraction from KaSAR308 image of vehicles and the corresponding picture acquired simultaneously by onboard camera is presented below (Figure 113).

Figure 113 : Picture acquired simultaneously with the SAR image (presented Figure 112) by onboard camera.

ROI N°	type of area	image	Polarization	incidence angle	Sigma0 (dB)	Sigma0 Contrast (dB)	Sigma0 (lin)	Sigma0 Std (lin)
V1	car	KaSAR304	Vv	39,83	-1,84	2,34	0,6546	1,0161
V2	car	KaSAR304	Vv	40,64	-3,14	1,04	0,4853	0,5455
V3	car	KaSAR304	Vv	40,53	-1,91	2,27	0,6442	0,7187
V4	car	KaSAR304	Vv	40,2	-3,44	0,74	0,4529	0,5181
V5	surrounding	KaSAR304	Vv	38,63	-4,18	0	0,3819	0,3819
V6	caravan	KaSAR107	Vv	23,46	-4,2	6,21	0,3802	0,6737
V7	caravan	KaSAR107	Vv	24,31	-6,88	3,53	0,2051	0,3917
V8	caravan	KaSAR107	Vv	26,74	-6,5	3,91	0,2239	0,4182
V9	caravan	KaSAR107	Vv	27,21	-7,26	3,15	0,1879	0,4089
V10	caravan	KaSAR107	Vv	34,99	-10,88	-0,47	0,0817	0,2274
V11	caravan	KaSAR107	Vv	35,58	-10,12	0,29	0,0973	0,1894
V12	surrounding	KaSAR107	Vv	21,89	-10,41	0	0,0910	0,1023
V13	caravan	KaSAR308	Vv	49,82	-8,7	7,59	0,1349	0,4277
V14	caravan	KaSAR308	Vv	51,36	-6,99	9,3	0,2000	1,4617
V15	caravan	KaSAR308	Vv	52,81	-7,08	9,21	0,1959	0,5946
V16	surrounding	KaSAR308	Vv	52,61	-16,29	0	0,0235	0,0256

We observe that at 30° incidence angle, the cars or motor homes are identified not because of contrast but more because of shape and shadows.

For larger incidence angle, the vehicles are presenting more contrast. This could be the result of two distinct effects. When the incidence increases, the backscatter of the sand decreases. The vehicles are composed of vertical surfaces which are going to interact more strongly with the incident wave when the incidence increases.

However, the cars located in the parking lot in St Gilles are still difficult to see.

3.4.6. Polarimetric behavior

The question of the polarimetric behavior of natural surfaces at Ka Band cannot be addressed with the KaSAR campaign as we acquired VV polarization only. However, on the RAMSES archive data, we did some acquisitions at HH and VV polarizations (not simultaneously but on the same flight). The images were post- processed in order to be in the same geometry and the result is presented in Figure 114 and Figure 115 as color-composite images. The color coding is Hh polarization on the red and the green channels, the Vv polarization on the Blue channel. They point out the similar behavior of Hh and Vv polarizations over natural landscape with an overall grey color. The coloring occurs primarily over the anthropogenic areas. This difference of behavior was observed in the RAMSES archive analysis where we observed that the histograms at HH had a larger shape than the VV histograms

Figure 114 : polarimetric color composed SAR Ka image (first part) from RAMSES data archive acquired over St Gilles. The color coding is: the red and green channels are 0610 Hh polarization and the blue channel is 0611 Vv polarization.

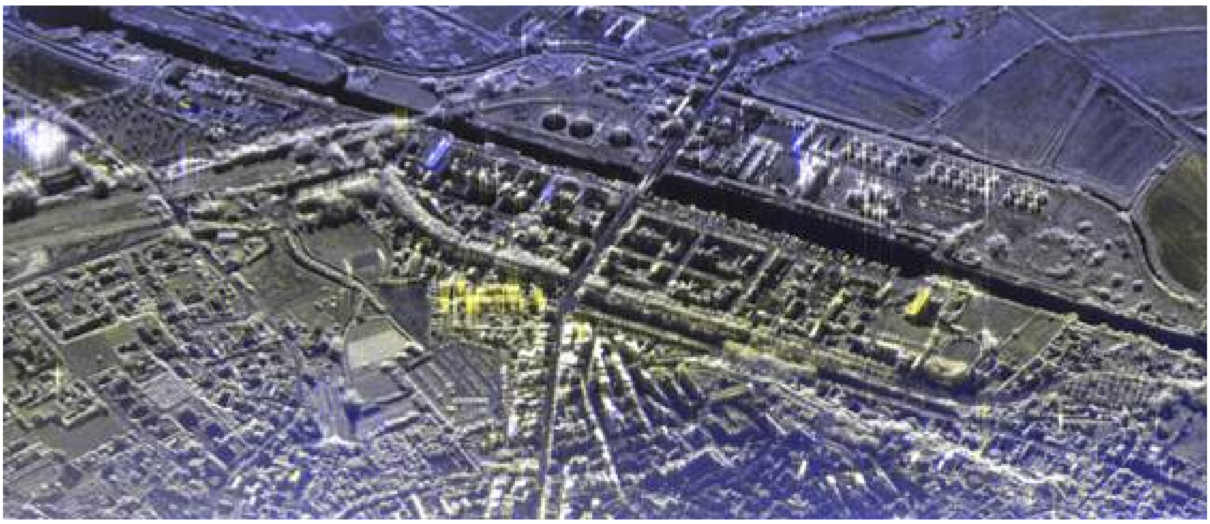

Figure 115 : polarimetric color composed SAR Ka image (second part) from RAMSES data archive acquired over St Gilles. The color coding is: the red and green channels are 0610 Hh polarization and the blue channel is 0611 Vv polarization.

4. Conclusions

The advantage of using Ka band is the possibility to get a large frequency allocation and potentially an interferometric system on a single platform due to the relatively small required baselines.
In the KaSAR project, we have explored the backscattering behavior of a large variety of targets with incidence angle.
The project had two main parts.
In the first part, we analyzed the RAMSES archive data acquired in 2008 at HH and VV polarization. In the second part, we acquired, processed, calibrated and analyzed VV Ka Band images from the DRIVE-BUSARD system. The simultaneous in-flight picture acquisition performed by the DRIVE-BUSARD has proven its interest for ground reporting.

We have structured the conclusion according to the objectives that were identified in the request for proposal from ESA.

<u>Agricultural area behavior</u>
Over the agricultural area around St Gilles, we have measured the sigma0 variation as a function of incidence angle. We observe that the sigma0 is almost constant with incidence angle at around -8dB (spread between -12dB to -5dB) across the range from 20 to 50°. Surprisingly, the trees or orchards do not have a significantly higher backscatter. The tree plots can be identified in the image mostly because of the texture inside the forest or the shadow on the edge of the trees. Comparing the July and September dates we did not observe a significant variation in backscatter over the different surfaces. The overall moisture conditions were equivalent, with a very dry soil on the three dates. The RAMSES archive data show more contrast over the area, and we believe this is linked to the fact that the area was more exploited in 2008 than nowadays. In 2012, most of the fields were not ploughed nor cultivated in June or September.
The polarimetric behavior was studied from the RAMSES archive data and a color composite image was formed between two acquisitions at respectively HH and VV polarizations acquired on the same day. The resulting image is not showing a strong coloring. Most fields are grey. The only areas showing a distinct behavior between HH and VV are the urban or industrial areas.
The measured sigma0 for short vegetation are significantly lower than the one provided by Mr Attema (**REF-7**). This is certainly linked to the large difference in the vegetated area conditions (South of France is very dry, so is the soil and the vegetation compared to the lush Netherland landscape)

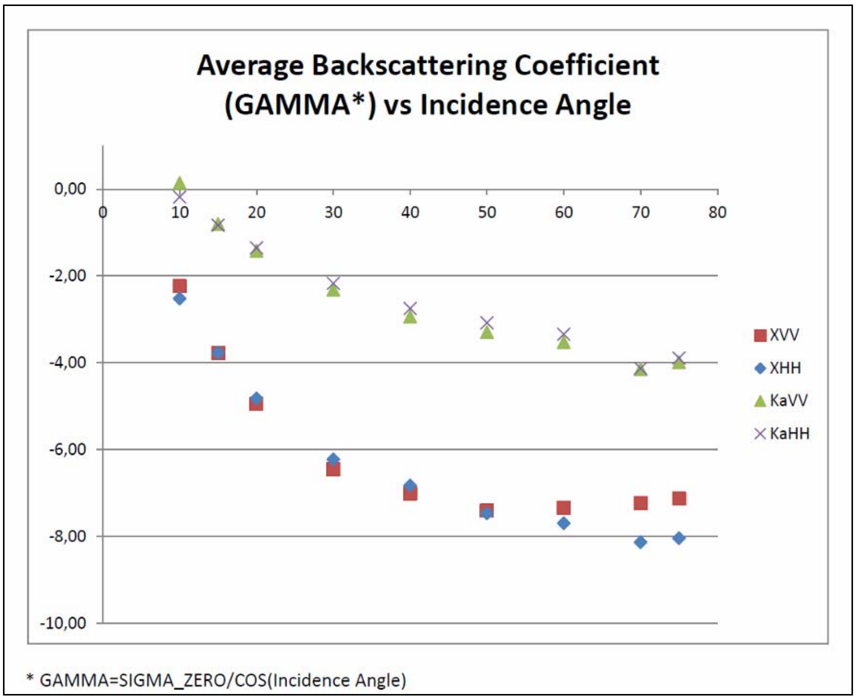

Figure 116 : Gamma0 value for short vegetation provided by Mr Attema

The measured sigma0 values over short vegetation are in agreement with the one presented in the reference book by Ulaby. The measured sigma0 for forest and trees are much higher than the values found in the Ulaby textbook.

The sea surfaces (sea and river)

The data set includes a variety of sea surfaces. On the RAMSES flight, the water surfaces were rough as it was windy. So was the weather on the first DRIVE-BUSARD flight. The second and third DRIVE-BUSARD flight occurred on very calm; smooth sea. We believe the sigma0 over the sea for these last two flights are at the noise level.

On the days corresponding to rougher sea, the radar images show clearly the wave pattern and its modulation to the sigma0. We can observe defocusing on the breaking wave next to the shore. The observed value ranges from -10dB for 20° incidence angle down to the noise level. (-30dB). The sigma0 values could certainly be stronger if the water surface gets rougher.

The sigma0's observed for the river are comparable to those over the sea.

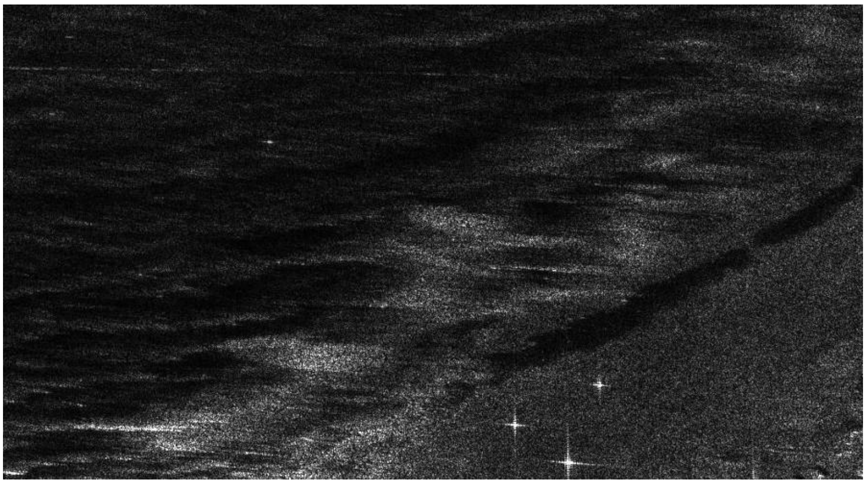

Figure 117 : defocusing effect on KaSAR107 slc image

Anthropogenic targets

Over industrial areas and urban areas, the radar-cross-sections are varying widely. A pixel can be very bright because of multiple bounce over the geometric structures while the neighboring pixel is in the shadow with a very low value. We have tried to quantify this high variability with histograms of radar cross-section in dB, of the 5x5 multi-look image. We have observed on the RAMSES data that the HH histogram is much wider than the VV histogram over the same features, and this behavior is illustrated in the color composite image where the coloring occurs mostly in yellow in the industrial areas.

Vehicles – boats - cars

The vehicles such as cars or caravans are barely visible in some images when they don't present any bright point scatterers. Their shape can be distinguished mostly because of their shadow. However, for larger incidence angle, the detection is better. The return from the vehicle is then constituted by more point scatterers and the background is also somewhat darker.

In the case of the large tankers (boats), the sharp and straight lines are creating strong returns and point scatterers from which the shape of the boat can be clearly established. This is certainly linked to the material of the hull: metallic in the case of the boats, plastic in the case of the motorhomes. Furthermore, the very straight lines found in the containers stored on the boats are creating some extremely strong return.